Demixing in free-burning arcs

A. B. Murphy
CSIRO Telecommunications and Industrial Physics, P.O. Box 218, Lindfield, New South Wales 2070, Australia
(Received 23 December 1996)

Demixing in atmospheric-pressure free-burning arcs is investigated using a two-dimensional numerical model that incorporates the combined diffusion coefficient treatment of diffusion. Arcs in mixtures of argon with helium, nitrogen, oxygen, and hydrogen are modeled. It is found that demixing almost always has a large influence on arc composition, with the greatest changes occurring in the argon-helium and argon-hydrogen arcs. The influence of three different demixing processes is assessed. Demixing due to frictional forces is found to dominate in the high-temperature regions of the arc, while demixing due to mole fraction gradients is important in the regions where dissociation of the molecular gases occurs. Demixing due to thermal diffusion has a smaller effect. The effects of demixing on arc temperature and flow velocity are usually small. The heat flux to the anode is significantly increased near the axis by demixing in argon-nitrogen and argon-hydrogen arcs. The predictions of the model are validated by comparison with spectroscopic measurements of arc composition in argon-nitrogen and argon-helium arcs. [S1063-651X(97)11205-3]

PACS number(s): 52.80.Mg, 52.25.Fi, 51.20.+d

I. INTRODUCTION

Mixtures of different gases are used in most industrial processes that utilize electric arcs. For example, in gas-tungsten arc welding (GTAW), mixtures of helium or hydrogen and argon are often used; in gas-metal arc welding, carbon dioxide or oxygen, or sometimes helium, hydrogen, or nitrogen, are added to argon; and air is commonly used as the plasma gas for plasma cutting. Other vapors may be derived from the vaporization of electrodes or droplets or particles. In processes such as plasma metallurgy and plasma waste destruction, very complicated gas mixtures occur.

It is not possible to assume that the relative concentrations of the gases present are uniform in the arc. This is obviously true when a source of one of the gases, for example metal droplets, is present in the arc. However, even in cases when the gases are fully mixed before being introduced into the arc region, a process known as demixing causes partial separation of the gases.

Demixing is a process driven by differences in the diffusion velocities of the species that are present in the arc. It occurs in the presence of temperature or pressure gradients, or of certain external forces such as electric fields. For example, since the degree of dissociation and ionization of a gas depends on the temperature, a temperature gradient can give rise to gradients in the mole fractions of the individual species present. These mole fraction gradients in turn drive diffusion until the sum of the forces, including those due to mole fraction gradients, frictional forces, thermal diffusion forces, and external forces, on the species is zero.

The initial observations of demixing in arcs were made as early as the beginning of the 20th century. Lenard [1] discovered the so-called *Lenardsche Hohlflammen* (Lenard's hollow flame), an electric arc in which the spectroscopic emission from metallic elements present in trace quantities was observed to be concentrated in a cylindrically symmetric zone separated from the central region. A summary of observations in such arcs was given by Eberhagen [2]. Eberhagen mistakenly explained the observations as a side effect of cataphoresis, the concentration of the metallic elements near the cathode due to the transport of ions in the electric field that is also observed in such arcs [3–6]. Frie [7] has pointed out the error in Eberhagen's reasoning.

Maecker [8] showed that demixing also took place for nonmetallic chemical elements, observing a concentration of fluorine on the axis of an SF_6 arc. Many of the observations of demixing that followed were made during measurements of atomic transition parameters, in which a knowledge of species densities was required. For example, Mastrup and Wiese [9] observed a concentration of helium on the axis of a helium-nitrogen arc, Roder [10] noted an increase in iron vapor concentration near the edge of an argon arc with $FeCl_3$ added, and Wobig [11] observed a decrease in the titanium to chlorine density ratio near the axis of arcs in nitrogen, argon, and helium to which $TiCl_4$ had been added. Schumaker and Popenoe [12] noted an increase in hydrogen concentration near the axis of an argon-hydrogen arc. Later, Schulz-Gulde and Barushka [13,14] observed demixing in an SF_6 arc in measurements of F I transition probabilities.

The first quantitative explanations of these demixing effects were contained in an important series of papers by Frie and Maecker, in which they classified and analyzed the significance of the different processes that drive demixing [7,15–17], and in a paper by Richter [18], who measured the degree of demixing in arcs in mixtures of argon, nitrogen, helium, and hydrogen, and explained the results in a similar manner to Frie and Maecker.

Sulfur hexafluoride arcs have continued to be studied extensively. Motschmann [19,20], Schulz-Gulde [21], and Vacquié [22] have assessed various methods of temperature and composition measurement in such arcs, and recently Gonzalez *et al.* [23] investigated the influence of demixing on the temperature of SF_6 arcs.

Most of the more recent studies of demixing have been related to the industrial applications of mixed gas plasmas. Vukanović and Vukanović [24,25] measured the effect of demixing in arcs used for spectrochemical analysis. Fischer [26] and Stormberg [27] measured and calculated the com-

position in high-pressure mercury–metal-halide discharge lamps; further measurements on such lamps were performed recently by Karabourniotis *et al.* [28]. Cheminat *et al.* [29] observed a demixing effect in measurements of the vaporization of a silver anode in an argon arc. Fincke and co-workers measured [30,31] and calculated [31] the influence of demixing in argon-helium plasma jets, and Hiraoka [32] observed a similar demixing effect in an argon-helium free-burning arc. Recently, Fudolig *et al.* [33] modeled temperature and concentration fields in an argon-nitrogen arc reactor, using an approach based on that presented here, and Suzuki *et al.* [34] and Snyder *et al.* [35] investigated the diffusion of small amounts of hydrogen added to argon arcs.

Only in a few of the above papers [26,27,31,33] were realistic models of the demixing process introduced. The main difficulty in calculating the effects of demixing is the need to treat the diffusion of the many different species present in mixed-gas plasmas. The conservation of mass of each of the species has to be considered, and diffusion coefficients describing the diffusion of each species with respect to every other species have to be calculated. Recently, Murphy [36] introduced the concept of combined diffusion coefficients, which allowed the treatment of diffusion to be greatly simplified for many mixed-gas plasmas. The concept was applied to a one-dimensional model of demixing in an argon-nitrogen arc [37], and to a two-dimensional model of demixing in argon-nitrogen and argon-helium arcs [38,39]. Not only does the concept simplify the mathematical treatment of demixing, but it also allows the respective influences of the different physical processes that drive demixing to be isolated.

The purpose of the work presented here is to investigate in detail the phenomenon of demixing in a range of gas mixtures relevant to industrial arc processes. A two-dimensional numerical model of the arc is used, with the combined diffusion coefficient formulation used to treat diffusion. Both the changes in composition caused by demixing, and the consequent changes in arc properties such as temperature, gas velocity, and thermal transport, are calculated. The contributions of the different demixing processes to the changes are assessed, and comparisons are made with experimental measurements.

In Sec. II the combined diffusion coefficient formulation is outlined, and its relation to the different demixing processes is demonstrated. Further, the equations and methods used in the computational model are presented. In Sec. III the results of the model are given for free-burning arcs in different mixtures of argon with helium, hydrogen, nitrogen, and oxygen. The predictions of the model are compared to available experimental data in Sec. IV. Conclusions are presented in Sec. V.

II. THEORY

A. Combined diffusion coefficient method

Diffusion in a gas can be described by equations for the mass flux $\mathbf{J}_i$, relative to the mass-average velocity, of each of the species i present. In a gas mixture containing q species, in the presence of a temperature gradient, the equations take the form [40,41]

$$\mathbf{J}_i \equiv m_i n_i \mathbf{v}_i = \frac{n^2}{\rho} m_i \sum_{j=1}^{q} m_j D_{ij} \mathbf{d}_j - D_i^T \nabla \ln T, \tag{1}$$

where $\mathbf{v}_i$ is the diffusion velocity of species i relative to the mass-average velocity and T is the temperature. The D_{ij} are ordinary diffusion coefficients, and the D_i^T are thermal diffusion coefficients. The term $\mathbf{d}_j$, given by

$$\mathbf{d}_j = \nabla x_j + \left(x_j - \frac{\rho_j}{\rho} \right) \nabla \ln P - \frac{\rho_j}{P\rho} \left(\frac{\rho}{m_j} \mathbf{F}_j - \sum_{l=1}^{q} n_l \mathbf{F}_l \right), \tag{2}$$

describes the diffusion forces due to gradients in mole fraction $x_j = n_j / n$ and pressure P, and due to external forces $\mathbf{F}_j$. n and ρ are, respectively, the number and mass densities of the gas mixture, and n_j, ρ_j, and m_j are, respectively, the number density, mass density, and mass of the jth species.

As can be seen from Eq. (1), there are q^2 ordinary diffusion coefficients and q thermal diffusion coefficients to be calculated; of these, $\frac{1}{2}q(q-1)$ and $q-1$, respectively, are linearly independent. A further complication that arises when charged particles are present is that the tendency of electrons to diffuse more rapidly than ions sets up an electric field, which influences the diffusion of all charged particles present. To take account of this effect, known as ambipolar diffusion, the diffusion coefficients have to be modified as shown by Devoto [41] and Murphy [36].

Murphy [36,42] has shown that in a mixture of two homonuclear gases that do not react with each other the treatment of diffusion can be greatly simplified if local chemical equilibrium is assumed. In this case, instead of considering the diffusion of individual species separately, one can consider the diffusion of gases. Here a gas, for example nitrogen, is defined to consist of all the species that can be derived from that gas, for example N_2, N_2^+, N, N^+, N^{2+}, and the electrons derived from the ionization of nitrogen molecules and atoms. It is possible to derive an expression for the mass flux of a gas, defined as the sum of the mass fluxes of all the species that make up the gas, that has the form

$$\overline{\mathbf{J}_A} = \frac{n^2}{\rho} \overline{m_A}\, \overline{m_B}\, \overline{D_{AB}^x} \nabla \overline{x_B} - (\overline{D_{AB}^{T1}} + \overline{D_A^T}) \nabla \ln T, \tag{3}$$

where $\overline{m_A}$ is the average mass of the heavy species of gas A, and $\overline{x_B}$ is the sum of the mole fractions of all species of gas B. Expressions for the combined mole fraction diffusion coefficient $\overline{D_{AB}^x}$ and the combined temperature diffusion coefficient $\overline{D_{AB}^{T1}}$, which are weighted averages of the ordinary diffusion coefficients, and the combined thermal diffusion coefficient $\overline{D_A^T}$, which is a weighted average of the thermal diffusion coefficients, have been given elsewhere [36,42]. The bar notation is used to denote that a variable refers to a gas rather than to a species. Gradients in the total pressure and external forces have been neglected in Eq. (3); if they were included a further combined diffusion coefficient would be required for the pressure gradient and for each external force considered. The reason that two distinct combined diffusion coefficients are derived from the ordinary diffusion coefficients is that the expression that describes the relation

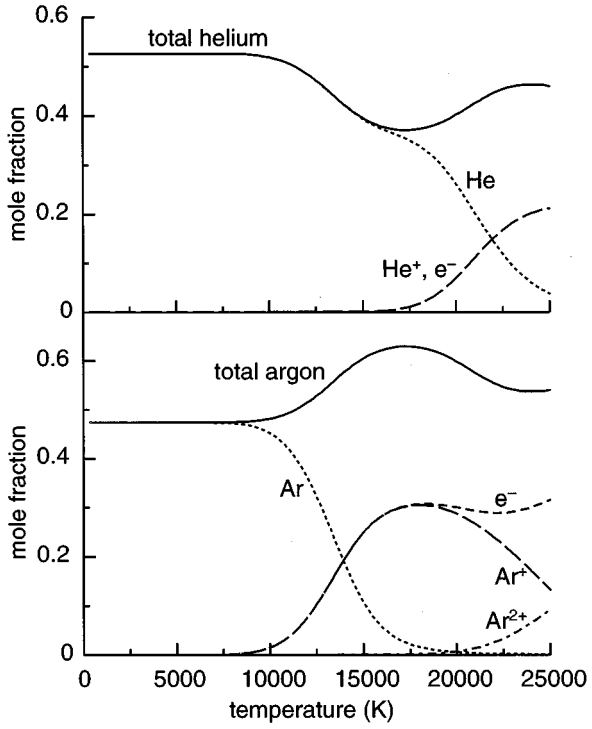

FIG. 1. Temperature dependence of the mole fractions of the species present in a mixture of argon and helium if no demixing occurs.

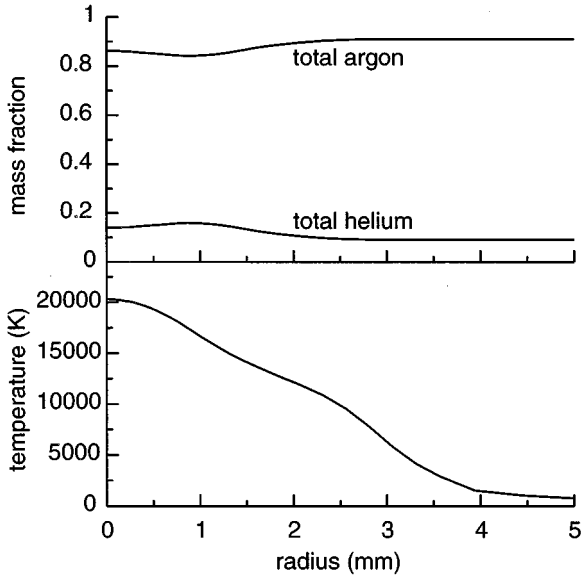

FIG. 2. Radial dependence of the total mass fractions of argon and helium for the mixture considered in Fig. 1, after the effects of demixing due to mole fraction gradients have been taken into account, for a typical arc temperature profile.

between the gradients of the mole fractions of the species and the gradient of the mole fraction of the gas has two terms:

$$\nabla x_j = (\partial x_j / \partial \overline{x_B}) \nabla \overline{x_B} + (\partial x_j / \partial T) \nabla T. \quad (4)$$

It should be noted that many authors have described diffusion in terms of gases rather than species in computational modeling of plasmas, but have done so in ways that introduce serious errors [42].

B. Classification of demixing processes

In their papers discussing the physical processes that lead to demixing, Frie and Maecker [7,17] classified these processes into a number of categories; demixing due to mole fraction (or partial pressure) gradients, frictional forces, thermal diffusion, and external forces. These categories may be elucidated by considering their effects in a mixture of two gases, for example argon and helium.

Figure 1 shows the mole fractions of each species present in the gas mixture as a function of temperature if demixing is neglected. It thus represents the composition that would be seen if the gas mixture were heated such that no gradients or external forces were present. At low temperature, only atoms are present. As the temperature increases above 10 000 K, the argon begins to ionize, each argon atom being replaced by an ion and an electron. Hence the total argon mole fraction $\overline{x_{\mathrm{Ar}}}$ increases and the total helium mole fraction $\overline{x_{\mathrm{He}}}$ decreases. This continues until a temperature of around 17 000 K is reached, at which point the helium atoms begin to ionize. Note that despite the changes in *mole* fraction with temperature, the *mass* fractions of the gases remain constant if demixing does not occur.

If we now consider the more realistic situation in which a temperature gradient is present, then the increase in $\overline{x_{\mathrm{Ar}}}$ and the decrease in $\overline{x_{\mathrm{He}}}$ represent mole fraction gradients. These, as shown in Eq. (3), drive diffusion of argon and helium until the mole fraction gradients no longer exist. This effect is known as demixing due to mole fraction gradients, and in this case leads to an increase in the *mass* fraction of helium in the high-temperature region, and an increase in the *mass* fraction of argon in the low-temperature region. Figure 2 shows the mass fraction as a function of radius for a typical arc temperature profile, calculated taking this process into account, for the same mixture considered in Fig. 1.

In general, demixing due to mole fraction gradients leads to an increase in the mass fraction of the chemical element with the higher ionization energy in the high-temperature region, or more precisely, in the region in which the temperature is such that one element is ionized and the other is not ionized.

A similar process occurs when a molecular gas is present. Dissociation of homonuclear diatomic molecules leads to each molecule being replaced by two atoms, and hence an increase in the mole fraction of the chemical element concerned. Demixing due to the resulting mole fraction gradient drives diffusion from the higher- to the lower-temperature region, leading to a decrease in the mass fraction of the element in the region in which it is dissociated.

Let us now consider the effect of the collisional interactions between the species on the demixing process, returning again to the example of argon and helium. We see from Fig. 1 that at temperatures between around 8000 and 17 000 K, argon is partially ionized so that the species Ar, Ar^+, and e^- are present, while helium is present almost solely as atomic helium. The mole fraction gradients of the respective species will drive a flux of argon atoms towards the region at

higher temperature, and a flux of argon ions and electrons towards the region at lower temperatures. These fluxes in themselves do not alter the composition if local chemical equilibrium can be assumed, since ionization and recombination reactions then occur sufficiently rapidly to balance the fluxes. However, helium atoms also collide with the argon species; the collisions with argon atoms drive the helium towards the higher-temperature regions, and the collisions with the argon ions and electrons drive the helium in the opposite direction. The net effect of the collisional interactions is to increase the mass fraction of helium in the regions at higher temperature. This effect is known as demixing due to frictional forces. Typically, but not always, it leads to an increase in the mass fraction of the lighter chemical element in the regions at higher temperature.

Thermal diffusion also leads to demixing whenever a temperature gradient is present. Usually, but again not always, thermal diffusion causes a flux of the lighter chemical element to regions at higher temperature. In the case of an argon-helium arc, demixing due to thermal diffusion further concentrates helium in the higher-temperature region.

All three demixing processes considered here act in the same direction in the case of a mixture of argon and helium. This is not always the case, and as will be seen, quite complicated mass fraction distributions can result from the competing influences of the different processes in some gas mixtures.

C. Demixing processes and the combined diffusion coefficients

Equation (3), which describes the diffusive mass flux of a gas in a mixture of two gases, can be written so that each term contains one of the combined diffusion coefficients:

$$\overline{\mathbf{J}_A}=\frac{n^2}{\rho}\overline{m_A}\,\overline{m_B}\,\overline{D_{AB}^{x}}\nabla\overline{x_B}-\overline{D_{AB}^{T1}}\nabla\ln T-\overline{D_A^T}\nabla\ln T. \tag{5}$$

Each term then corresponds to one of the three demixing processes defined in Sec. IIB. This can be demonstrated by considering the equilibrium situation, in which the mass fluxes of the gases have vanished. The equilibrium mole fraction gradients of the two gases are calculated by setting $\overline{\mathbf{J}_A}=\mathbf{0}$ in Eq. (5), giving

$$\nabla\overline{x_B}=-\nabla\overline{x_A}=\frac{\rho}{n^2}\frac{(\overline{D_{AB}^{T1}}+\overline{D_A^T})\nabla\ln T}{\overline{m_A}\,\overline{m_B}\overline{D_{AB}^{x}}}. \tag{6}$$

By setting $\overline{D_{AB}^{T1}}=\overline{D_A^T}=0$, we obtain $\nabla\overline{x_B}=\nabla\overline{x_A}=\mathbf{0}$, which is simply the condition that mole fraction gradients have vanished; hence demixing due to mole fraction gradients is described by the term in the remaining nonzero diffusion coefficient $\overline{D_{AB}^{x}}$, which is termed the combined mole fraction diffusion coefficient.

The term in the combined thermal diffusion coefficient $\overline{D_A^T}$ describes demixing due to thermal diffusion, since this is the only term in which the thermal diffusion coefficients are involved. The term in the remaining diffusion coefficient, the combined temperature diffusion coefficient $\overline{D_{AB}^{T1}}$, describes demixing due to the remaining phenomenon treated in the equations, that is, due to frictional forces.

The one-to-one correspondence between combined diffusion coefficients and demixing processes allows the contribution of each process to be calculated separately, thereby allowing the physical causes of demixing to be examined. If other demixing processes, such as demixing due to gradients in the total pressure or due to an external field, were considered, there would be a further combined diffusion coefficient corresponding to each process.

D. The arc model

The free-burning arc model used in this work is based on a two-dimensional axisymmetric model of a single-gas arc [43]. It has been extended to allow arcs in mixtures of two gases to be treated by inclusion of an equation for the conservation of mass of one of the gases, and by modifying the energy conservation equation to take into account changes in enthalpy due to diffusion of the gases.

It is assumed that the arc is in local thermodynamic equilibrium, and that the plasma flow is laminar. The temperature of the cathode surface is defined using experimental data, but the computational region for the calculation of current density includes the cathode as well as the arc column. The equations solved follow.

Mass conservation:

$$\nabla\cdot(\rho\mathbf{v})=0. \tag{7}$$

Momentum conservation:

$$\nabla\cdot(\rho\mathbf{v}\mathbf{v})=-\nabla P-\nabla\cdot\overleftrightarrow{\tau}+\rho\mathbf{g}, \tag{8}$$

where the nonzero components of the stress tensor $\overleftrightarrow{\tau}$ are

$$\tau_{rr}=-2\,\eta\partial v_r/\partial r, \tag{9}$$

$$\tau_{\theta\theta}=-2\,\eta v_r/r, \tag{10}$$

$$\tau_{zz}=-2\,\eta\partial v_z/\partial z, \tag{11}$$

and

$$\tau_{zr}=\tau_{rz}=-\eta(\partial v_z/\partial r+\partial v_r/\partial z). \tag{12}$$

Energy conservation:

$$\nabla\cdot(\rho\mathbf{v}h)=\frac{\mathbf{j}^2}{\sigma}-U+\nabla\cdot\left(\frac{\kappa}{c_p}\nabla h\right)+\frac{5k}{2ec_p}\mathbf{j}\cdot\nabla h+\nabla\cdot\left[(\overline{h_A}-\overline{h_B})\left(\overline{\mathbf{J}_A}-\frac{\kappa}{c_p}\nabla\overline{Y_A}\right)\right]. \tag{13}$$

Mass conservation of one gas:

$$\nabla\cdot(\rho\mathbf{v}\overline{Y_A})=-\nabla\cdot\overline{\mathbf{J}_A}. \tag{14}$$

Electric current continuity:

$$\nabla\cdot\mathbf{j}=0, \tag{15}$$

where

$$\mathbf{j}=-\sigma\nabla\phi. \tag{16}$$

Maxwell's equation:

$$\nabla \times \mathbf{B} = \mu_0 \mathbf{j}. \tag{17}$$

In the above equations, $\mathbf{v}$ is the mass-average velocity of the gas, with radial and axial components v_r and v_z, respectively, P is the pressure, $\mathbf{j}$ is the current density, ϕ is the electric potential, $\mathbf{B}$ is the magnetic field induced by the current, h is the plasma enthalpy, and $\overline{Y_A}$ is the total mass fraction of gas A, defined as the sum of the mass fractions of the species of gas A. The material functions are mass density ρ, viscosity η, net radiative emission coefficient U, thermal conductivity κ, specific heat at constant pressure c_p, and electrical conductivity σ. All these material functions are functions of temperature and the respective mass fractions of gases A and B. $\overline{h_A}$ and $\overline{h_B}$ are, respectively, the enthalpies of gas A and gas B, defined as the sum of the enthalpies of the species making up the respective gas, and are functions of temperature only. Constants appearing in the equations are the acceleration due to gravity $\mathbf{g}$, Boltzmann's constant k, the electronic charge e, and the permeability of free space μ_0.

The second last term in Eq. (13), which was omitted by Lowke *et al.* [43], describes energy transfer due to the flow of electrons and is generally included in arc models. The last term describes the change in enthalpy due to the diffusive mixing of gases A and B.

The mass flux $\overline{\mathbf{J}_A}$, which appears in Eqs. (13) and (14), is given in Eq. (3) in terms of the gradient of the mole fraction $\overline{x_A}$. It may be written in terms of $\overline{Y_A}$ by using $x_A = (M/\overline{M_A})Y_A$, where M and $\overline{M_A}$ are the masses averaged over all species, including electrons, of the gas mixture and of gas A, respectively.

The thermodynamic properties h, c_p, and ρ were calculated as a function of temperature and $\overline{Y_A}$ for the gas mixtures considered using the NASA code [44,45]. The transport coefficients η, κ, σ, $\overline{D_{AB}^x}$, $\overline{D_{AB}^{T1}}$, and $\overline{D_A^T}$ were calculated as described by Murphy and Arundell [46] for argon-nitrogen and argon-oxygen mixtures, by Snyder *et al.* [35] for argon-hydrogen mixtures, and by Murphy [47] for argon-helium mixtures. Net radiative emission coefficients U for argon, helium, oxygen, and hydrogen were calculated using the method of Cram [48]. Those for nitrogen were calculated by taking the values of Ernst *et al.* [49] for a plasma radius of 1.5 mm, and multiplying these by a factor of 1.5 because the radius of the radiating central region of the arc is less than 1.5 mm [50].

The coupled partial differential equations describing the arc were solved numerically using the control volume approach of Patankar [51], incorporating the modifications recommended by Van Doormal and Raithby [52]. A rectangular grid of 82 axial by 48 radial cells was used, with the grid more closely spaced near the electrodes. Comparison with results obtained with a 41 by 24 grid showed a maximum change of 8% in the mass fraction of the minority gas, and generally much less.

The boundary conditions for all variables except $\overline{Y_A}$ have been given by Lowke *et al.* [43], and will not be repeated here. On axis the condition $\partial \overline{Y_A}/\partial r = 0$ is imposed to account for axisymmetry. At the anode, the gradient boundary condition $\partial \overline{Y_A}/\partial z = 0$ is used. At the top and radial edge boundaries, and at the cathode, $\overline{Y_A}$ is chosen to be equal to its value for the input gas mixture, since a free-burning arc is shielded from the atmosphere by this gas.

Some care has to be taken in treating diffusion close to the electrodes, since the large difference in temperature between the electrode and the arc causes the diffusive mass flux term $\overline{\mathbf{J}_A}$ in Eq. (14) to become unrealistically large in the control volumes adjacent to the electrodes, as is clear from Eq. (3). The gradients in the sheath are in fact so large that the assumption of local thermodynamic equilibrium is not valid, and the equations used in the model are not applicable. The problem is circumvented by setting $\overline{\mathbf{J}_A}$ to zero in the control volumes adjacent to the electrodes and in their nearest neighbors.

It was shown in Sec. II C that the different demixing processes correspond to the different combined diffusion coefficients. By setting the respective coefficients to zero in Eq. (3), with which the variable $\overline{\mathbf{J}_A}$ in Eqs. (13) and (14) is calculated, it is possible to isolate the influence of the different processes on the change in arc composition due to demixing. It is also instructive to calculate arc properties such as temperature, velocity, and heat fluxes in the absence of demixing, that is, when $\overline{Y_A}$ is uniform throughout the arc. This can be achieved by removing Eq. (14) from the model, and setting the final term in Eq. (13) to zero.

III. RESULTS

An arc typical of those used in gas-tungsten arc welding was modeled, with a cathode of 3.2 mm diameter and a conical tip of 60° included angle situated 5 mm above a flat anode (or workpiece). The arc current was 200 A, and the total input gas flow was 10 L min^{-1}. The gas mixture was input through a nozzle of radius 2.35 mm, concentrically around the cathode.

In the following subsections, the effects of demixing are examined for arcs in mixtures of argon with helium, nitrogen, oxygen, and hydrogen. The changes in mass fraction are calculated for a range of input compositions, and the contributions of the different demixing processes are assessed. These contributions are related to the combined diffusion coefficients for the mixtures. By calculating the temperature and velocity fields and the heat flux to the anode, both while including and while neglecting the effects of demixing, the influence of demixing on these parameters can be determined.

A. Argon-helium arcs

Mixtures of argon and helium are relatively simple in demixing terms since they are both atomic gases, so dissociation effects do not have to be considered. Also, as noted in Sec. II B, all demixing processes act in the same direction, to increase the helium mass fraction in the regions at higher temperature.

Figure 3 shows the distribution of helium and the temperature distribution in an arc in a mixture of 10% helium and 90% argon by mass, corresponding to 52.6% helium by mole. The mass fraction of helium in the hottest regions of the arc is over 2.5 times larger than in the input gas, demonstrating that demixing can generate large changes in arc com-

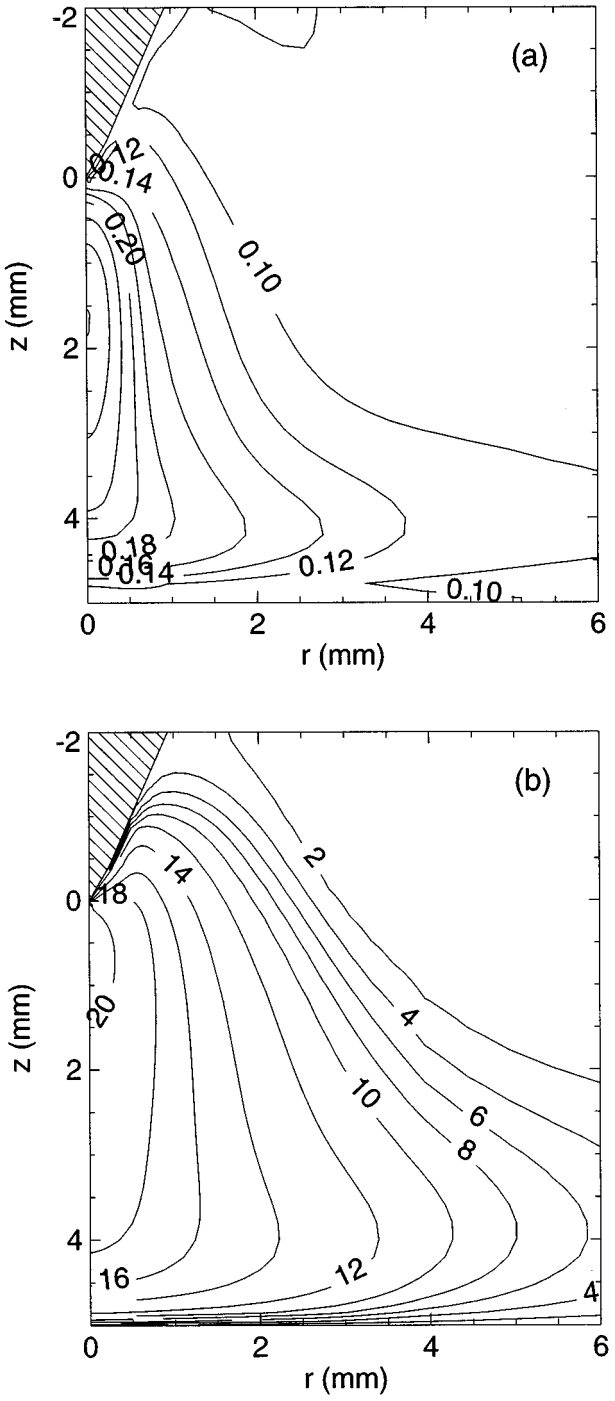

FIG. 3. (a) Isopleths of helium mass fraction and (b) isotherms, labeled in units of 1000 K; calculated for a 200 A 5 mm arc with a 10 L min^{-1} input flow composed of 10% helium and 90% argon by mass.

position. The mass fraction contours are similar in shape to the temperature contours, indicating that the helium mass fraction increases monotonically with temperature.

Figure 4 shows the calculated radial dependence of the mass fraction at four axial positions in arcs in three different mixtures of argon and helium, 1%, 5%, and 10% helium by mass, corresponding to 9.2%, 35.5%, and 52.6% by mole. The greatest percentage increase in the helium mass fraction occurs in the last case, but in all cases the helium mass fraction is more than doubled in the hottest regions of the arc.

The influence of the different demixing processes is shown in Fig. 5. As noted above, all three demixing processes considered lead to the concentration of helium near the arc axis. Demixing due to mole fraction gradients has only a relatively small effect, causing an increase in the helium mass fraction of up to about 30%. The increase occurs at radii of less than 2 mm, corresponding to temperatures above 12 500 K, at which argon atoms are becoming ionized. At radii of less than 1 mm, corresponding to temperatures above 17 000 K, helium atoms also start to become ionized, and the magnitude of the demixing due to mole fraction gradients decreases.

The most important effect is demixing due to frictional forces, which causes the helium mass fraction to increase from a radius of around 2 mm right up to the arc axis. Demixing due to thermal diffusion also has a significant effect, particularly close to the arc axis.

To gain a more fundamental understanding of the influence of demixing, it is useful to examine the dependence of the three combined diffusion coefficients on temperature and composition. The combined diffusion coefficients are plotted against temperature in Fig. 6 for three different mixtures of argon and helium. The combined mole fraction diffusion coefficient is always positive, and does not depend as strongly on gas composition as the other two combined diffusion coefficients. It is largest in the temperature range in which ions and neutrals are present in roughly equal numbers (cf. Fig. 1); the large size of the Coulomb collision cross section ensures that it decreases when the collisions between charged species dominate [46]. The combined temperature diffusion coefficient may be either positive or negative, depending on the net effect of the interactions between all the species present. Typically, but not always, it is found that $\overline{D_{AB}^{T1}}>0$ in a mixture of gases A and B if $\overline{m_A}>\overline{m_B}$. Equation (6) indicates that when $\overline{D_{AB}^{T1}}$ is positive, demixing due to frictional forces will increase the mass fraction of gas B in the regions at higher temperature. The combined thermal diffusion coefficient may also be positive or negative; it is usually the case that $\overline{D_A^T}>0$ in a mixture of gases A and B if $\overline{m_A}>\overline{m_B}$.

Figure 6 shows that $\overline{D_{\mathrm{Ar,He}}^{T1}}>0$ and $\overline{D_{\mathrm{Ar}}^{T}}>0$ for all mixtures of argon and helium, except for $\overline{D_{\mathrm{Ar}}^{T}}$ for a high helium mass fraction and high temperature. This explains the concentration of helium in the arc center, caused by demixing due to frictional forces and thermal diffusion, that is shown in Fig. 5.

B. Argon-nitrogen arcs

Arcs in mixtures of argon and nitrogen exhibit more complicated demixing behavior than those in argon and helium mixtures, both because nitrogen is a diatomic gas, and because the influence of frictional forces on demixing is more complex.

Figure 7 shows the distribution of nitrogen and the temperature distribution in an arc in a mixture of 20% nitrogen and 80% argon by mass, corresponding to 26.2% molecular nitrogen by mole. It is clear that demixing again leads to substantial changes in arc composition,

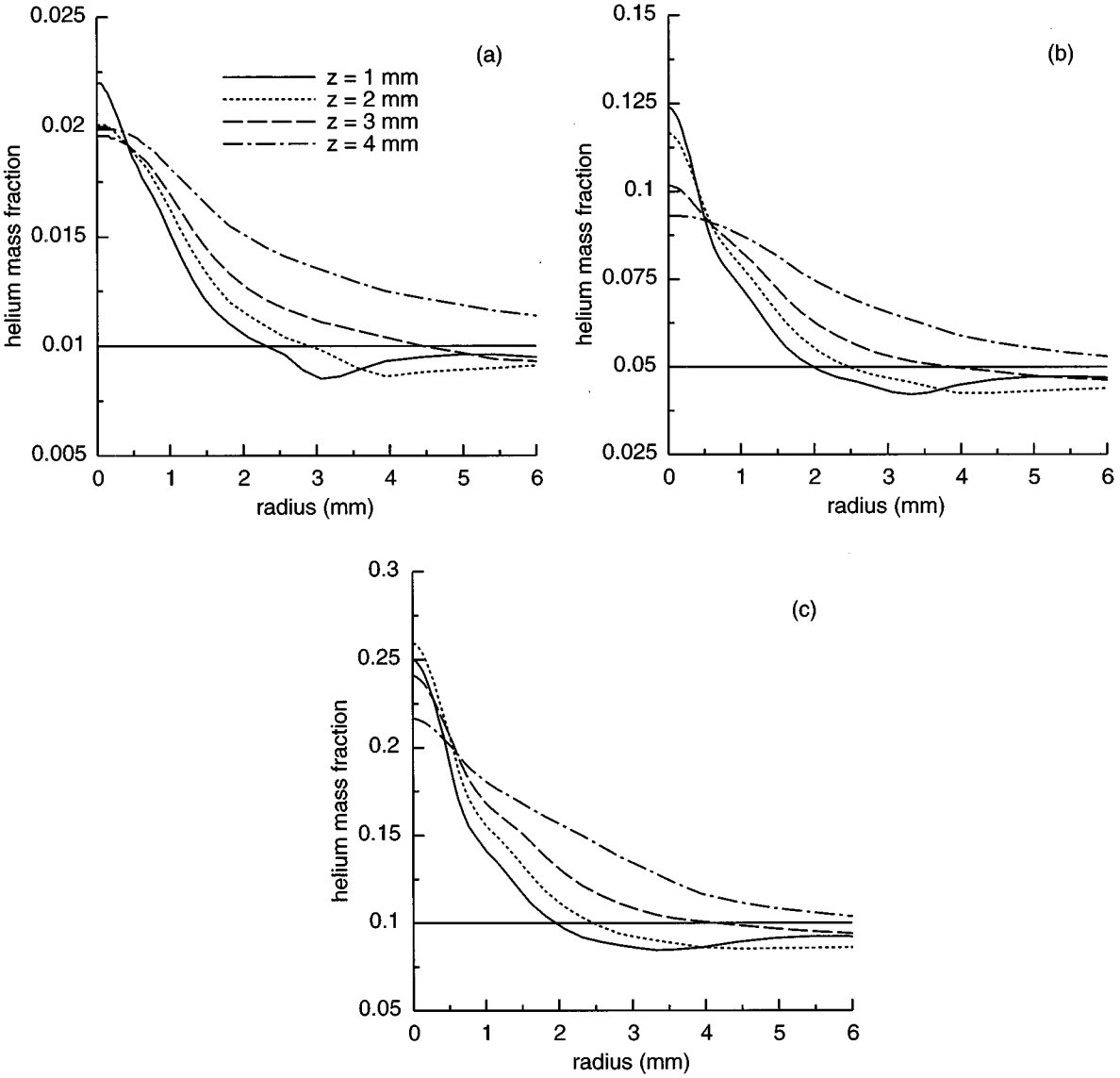

FIG. 4. Radial dependence of the mass fraction of helium gas at four axial distances below the cathode, for a 200 A 5 mm arc with a 10 L min^{-1} input flow composed of (a) 1% helium and 99% argon; (b) 5% helium and 95% argon; (c) 10% helium and 90% argon by mass. The horizontal line shows the input mass fraction.

although the changes are smaller than in the argon-helium arc. The mass fraction of nitrogen increases near the arc axis, but decreases at larger radii, at temperatures close to that at which nitrogen molecules dissociate. The peak value of the nitrogen mass fraction occurs near the anode, rather than in the higher-temperature region near the cathode as was found for the helium mass fraction in the argon-helium arc.

This behavior is investigated further in Fig. 8, which shows the radial dependence of the nitrogen mass fraction for three different mixtures of argon and nitrogen; 20%, 45%, and 75% nitrogen by mass, corresponding to 26.2%, 53.8%, and 81.1% by mole, respectively. Three distinct features are apparent in the figures. First, in all cases, there is a small increase followed by a larger decrease in the nitrogen mass fraction as the radius decreases from 6 to 2 mm, the peak and subsequent dip occurring at smaller radii at axial positions closer to the cathode. This is caused by demixing due to mole fraction gradients associated with the dissociation of nitrogen molecules, which occurs at temperatures between about 6000 and 7000 K. As noted in Sec. II B, dissociation of molecules causes an increase in the mole fraction. The resulting mole fraction gradient drives a flux of nitrogen towards the regions at lower temperature, where the nitrogen atoms are recombined.

The second feature is a change in the nitrogen mass fraction at radii less than about 1.5 mm. In Fig. 8(a), there is a large increase in the nitrogen mass fraction in this region, in Fig. 8(c), there is a large decrease, and in Fig. 8(b), there is only a minor change. These effects are chiefly a result of demixing due to frictional forces, as will be shown below. In the case of an argon-nitrogen mixture, demixing due to frictional forces can act in different directions depending on the relative mass fractions of the two gases. If the mass fraction of nitrogen is small, the demixing causes an increase in the nitrogen mass fraction, whereas if it is large, demixing causes it to decrease. At intermediate nitrogen mass fractions, demixing has little effect.

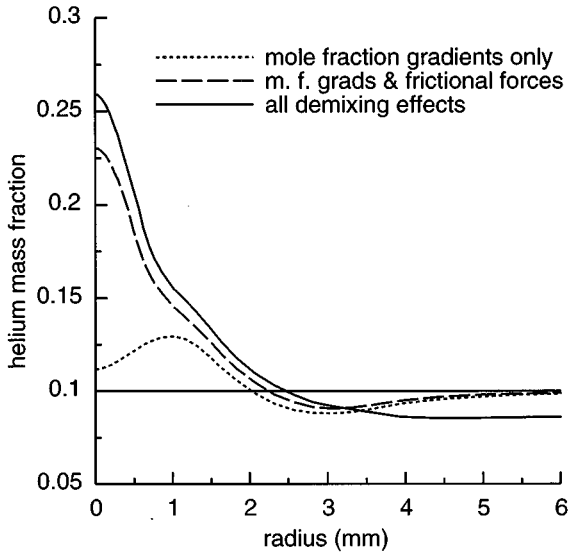

FIG. 5. Calculated radial dependence of the mass fraction of helium 2 mm below the cathode for the conditions of Fig. 3, with the effects of the different demixing processes shown.

The final feature apparent in Fig. 8 is a change in the nitrogen mass fraction in the central 0.5 mm towards its value in the input gas stream. This change is generally greatest close to the cathode, and is a result of the large axial flow velocity close to the arc axis. Diffusion is not sufficiently rapid to allow complete demixing of the input gas mixture in this region, due to the rapid convective influx of the input gas mixture. This effect is not nearly so marked in the argon-helium arc, since helium diffuses much more rapidly than nitrogen, and since the flow velocity is smaller in the argon-helium arc (see Sec. III E).

Figure 9 shows the influence of the different demixing processes on the composition of the argon-nitrogen arc. Demixing due to mole fraction gradients is found to lead to a very strong shift of nitrogen towards the edge of the arc at regions around a radius of 2.5 mm, corresponding to the dissociation temperature of nitrogen. In the central region of the arc, where the gases ionize, there is relatively little demixing due to mole fraction gradients. This is because argon and nitrogen atoms have similar ionization energies, so large mole fraction gradients of the gases are not set up by ionization. Demixing due to frictional forces is found to have a much stronger influence in the central regions, strongly concentrating nitrogen near the arc axis in this case. It also decreases the changes in composition caused by demixing due to mole fraction gradients in the regions near the dissociation temperature of nitrogen. Demixing due to thermal diffusion is found to have a relatively small effect; as in the argon-helium arc, it concentrates the lighter gas in the higher-temperature regions.

Figure 10 shows the combined diffusion coefficients for different mixtures of argon and nitrogen. The most interesting feature is that the combined temperature diffusion coefficient $\overline{D^{T1}_{\mathrm{Ar,N}}}$ changes sign depending on the relative concentrations of the two gases. This explains the dependence of direction of demixing on the gas composition that was noted in the discussion of Fig. 8; Eq. (6) indicates that the mass fraction of gas B will increase as temperature increases if

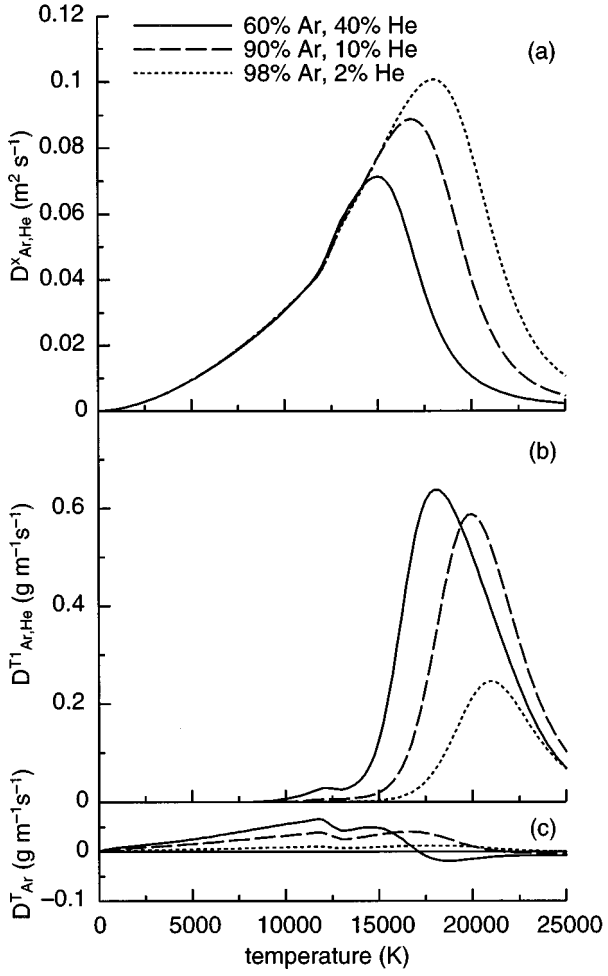

FIG. 6. Combined diffusion coefficients for different mixtures of argon and helium by weight. (a) Combined mole fraction diffusion coefficient; (b) combined temperature diffusion coefficient; (c) combined thermal diffusion coefficient.

$\overline{D^{T1}_{AB}}>0$ and decrease if $\overline{D^{T1}_{AB}}<0$ (assuming $|\overline{D^{T}_{A}}|\ll|\overline{D^{T1}_{AB}}|$, as is the case here).

C. Argon-oxygen arcs

Arcs in mixtures of argon and oxygen exhibit broadly similar behavior to those in argon and nitrogen mixtures. Figure 11 shows the distribution of oxygen and the temperature distribution in an arc in a mixture of 20% oxygen and 80% argon by mass, corresponding to 23.8% molecular oxygen by mole. A substantial change in arc composition is again observed; the oxygen mass fraction increases by more than 50% near the arc axis. This increase is larger than that observed for nitrogen in the argon-nitrogen arc, but the shape of the contours is similar; in particular, the mass fraction of oxygen is largest on axis near the anode, and it decreases at larger radii, where temperatures fall below the dissociation temperature of oxygen.

Figure 12 shows the radial dependence of the oxygen mass fraction for three different mixtures of argon and oxygen; 5%, 20%, and 80% oxygen by mass, corresponding to 6.2%, 23.8%, and 83.3% by mole, respectively. The three main features that were noted in the argon-nitrogen arcs are also apparent in the argon-oxygen arcs. First there is the

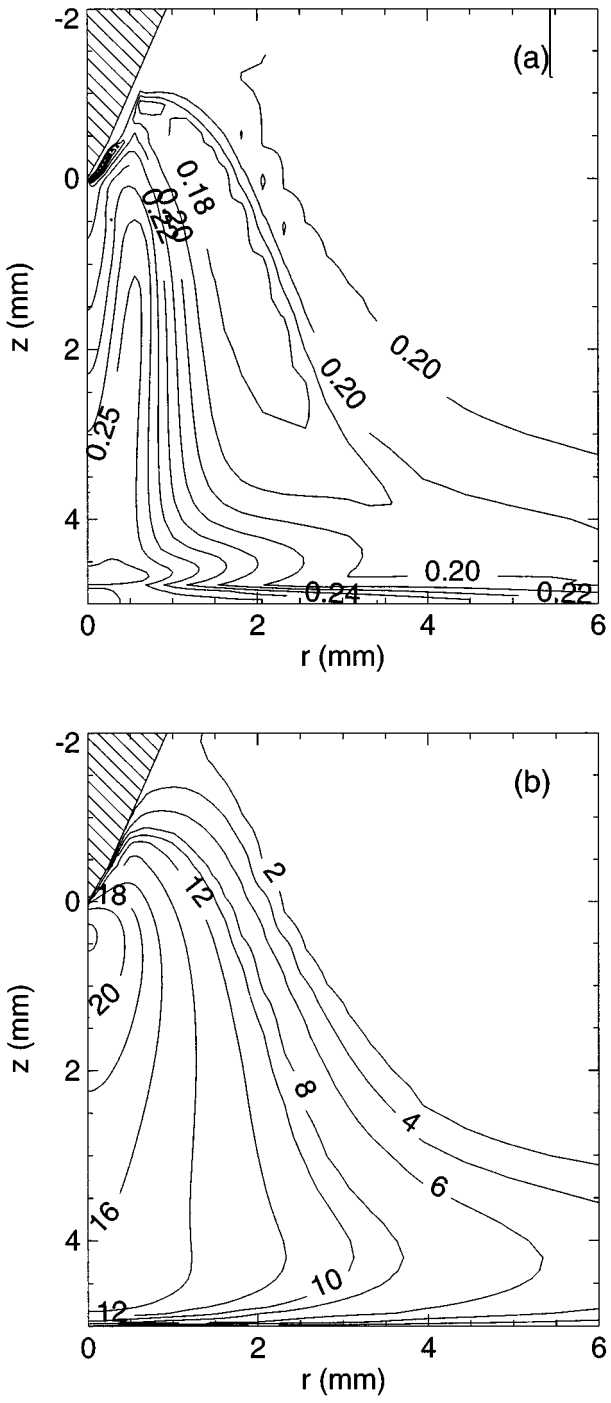

FIG. 7. (a) Isopleths of nitrogen mass fraction and (b) isotherms, labeled in units of 1000 K; calculated for a 200 A 5 mm arc with a 10 L min^{-1} input flow composed of 20% nitrogen and 80% argon by mass.

small increase followed by a sharp decrease in the oxygen mass fraction as the radius decreases from 6 to 2.5 mm, caused by demixing due to the mole fraction gradients associated with the dissociation of oxygen molecules, which occurs at temperatures between around 3000 and 3500 K. The second feature is the change in the oxygen mass fraction at radii less than about 1.5 mm. In Figs. 12(a) and 12(b), a large increase in the oxygen mass fraction occurs, but in Fig. 12(c), there is a decrease. As in the argon-nitrogen mixture, demixing due to frictional forces acts in different directions depending on the mass fractions of the two gases. The final feature apparent in Fig. 12 is the change in the oxygen mass fraction in the central 0.5 mm towards its value in the input gas stream, due to the large axial flow velocity close to the arc axis. As can also be seen in Fig. 11, the effect is larger near the cathode; demixing has a greater effect near the anode since diffusion has had a longer time to occur.

Figure 13 shows the influence of the different demixing processes on the composition of the argon-oxygen arc. Again the results are similar to those calculated for the argon-nitrogen arc, shown in Fig. 9. Since oxygen is a molecular gas, demixing due to mole fraction gradients is observed in regions at temperatures close to the dissociation temperature of oxygen, at radii around 3 mm, leading to a displacement of oxygen towards the edge of the arc. Further, since oxygen, like nitrogen, has a similar ionization energy to argon, there is again little demixing due to mole fraction gradients in the high-temperature regions. Demixing due to frictional forces and thermal diffusion both concentrate oxygen near the arc axis in this case. The effect is greater than in the argon-nitrogen arc for both these demixing processes.

Figure 14 shows the combined diffusion coefficients for different mixtures of argon and oxygen. The combined temperature diffusion coefficient $\overline{D^{T1}_{\mathrm{Ar,O}}}$ changes sign depending on the relative concentrations of the two gases, as did $\overline{D^{T1}_{\mathrm{Ar,N}}}$ for the argon-nitrogen mixture. In the case of the argon-oxygen mixture, the sign change occurs for an oxygen mass fraction of around 0.6, compared to a nitrogen mass fraction of around 0.45 for the argon-nitrogen mixture. The magnitude of $\overline{D^{T1}_{\mathrm{Ar,O}}}$ is generally larger than that of $\overline{D^{T1}_{\mathrm{Ar,N}}}$; this leads to the stronger demixing effects observed in the argon-oxygen arc.

D. Argon-hydrogen arcs

The results presented so far may be divided into two groups; those pertaining to the relatively heavy molecular gases nitrogen and oxygen, and those pertaining to the light atomic gas helium. Hydrogen is both light and molecular, so it might be expected that demixing in argon-hydrogen arcs will share some of the characteristics observed in the arcs in the different gas mixtures treated so far.

Figure 15 shows the distribution of hydrogen and the temperature distribution in an arc in a mixture of 5% hydrogen and 95% argon by mass, corresponding to 51.1% molecular hydrogen by mole. The hydrogen mass fraction increases to twice its input value near the anode on the arc axis, which is a similarly large increase to that found for helium. The shape of the contours is similar to those calculated for oxygen and nitrogen, however. It is again observed that there is a decrease in the mass fraction of the molecular gas at large radii, near its dissociation temperature.

The radial dependence of the hydrogen mass fraction is shown in Fig. 16 for three different mixtures of argon and hydrogen; 0.5%, 1%, and 5% hydrogen by mass, corresponding to 9.1%, 16.7%, and 51.1% by mole, respectively. Three features that were noted in the argon-nitrogen and argon-oxygen arcs are again apparent. The increase followed by a decrease in the molecular gas mass fraction as the radius decreases from the edge to 2.5 mm again occurs because of

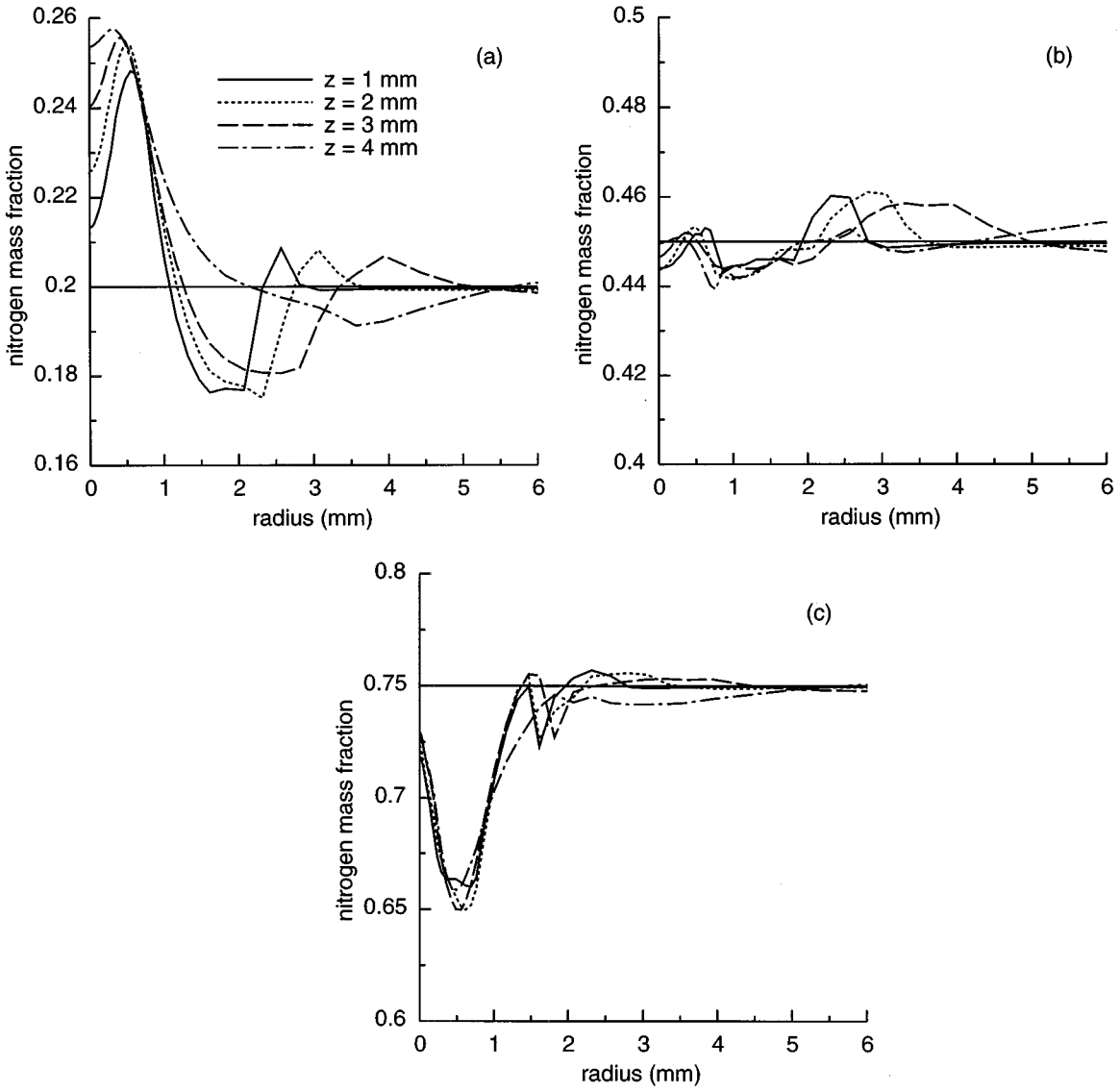

FIG. 8. Radial dependence of the mass fraction of nitrogen gas at four axial distances below the cathode, for a 200 A 5 mm arc with a 10 L min^{-1} input flow composed of (a) 20% nitrogen and 80% argon; (b) 45% nitrogen and 55% argon; (c) 75% nitrogen and 25% argon by mass. The horizontal line shows the input mass fraction.

demixing due to mole fraction gradients associated with the dissociation of hydrogen molecules, which occurs at temperatures between about 3000 and 3500 K. The argon-hydrogen arc is somewhat broader than the argon-nitrogen and argon-oxygen arcs (cf. Figs. 8, 12, and 16), so this feature occurs at larger radii. The second feature, the change in the mass fraction near the arc axis, also occurs at larger radii in the argon-hydrogen arc, extending out to about 3 mm at an axial position of 4 mm below the cathode. The hydrogen mass fraction reaches more than three times its input value for the 0.5% and the 1% hydrogen arcs, which confirms the general trend that the larger the difference in masses of the input gases, the larger the effect of demixing. (This is not an absolute rule, as is illustrated by the result that the mass fraction change in the argon-oxygen arc is larger than in the argon-nitrogen arc.)

The final feature apparent in Fig. 16 is the change in the hydrogen mass fraction in the central 0.5 mm towards its value in the input gas stream, due to the large axial flow velocity close to the arc axis. This effect is more marked when the hydrogen concentration is larger, because the flow velocity is greater. The same effect was also seen for the other molecular gases, but not for the argon-helium arc. There are two reasons for this. The first is that the flow velocity on the axis of the argon-helium arc is lower than in the other arcs (see Sec. III E). The second is that diffusion coefficients, and hence the rate of diffusion, for the argon-helium mixture are larger than for the other mixtures, particularly at the high temperatures found near the arc axis. The diffusion coefficients for the argon-hydrogen mixture are lower than for the argon-helium mixture, despite the inverse relationship between diffusion coefficient and mass; the reasons for this will be discussed below.

Figure 17 shows the influence of the different demixing processes on the composition of the argon-hydrogen arc. The influence of demixing due to mole fraction gradients and due to frictional forces is similar to that seen in the argon-nitrogen and argon-oxygen arcs. However, demixing due to

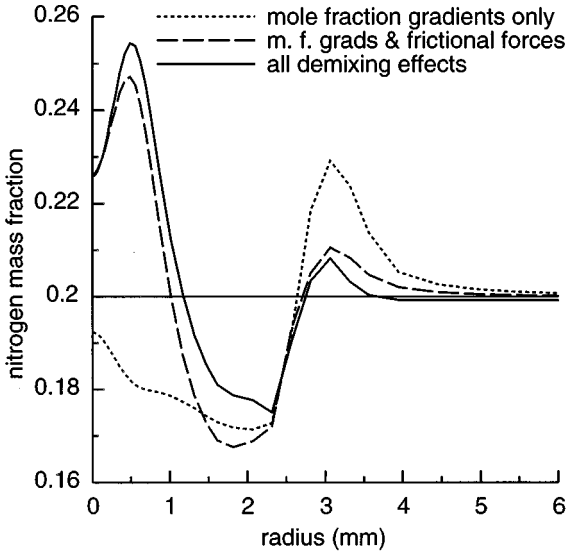

FIG. 9. Calculated radial dependence of the mass fraction of nitrogen 2 mm below the cathode for the conditions of Fig. 7, with the effects of the different demixing processes shown.

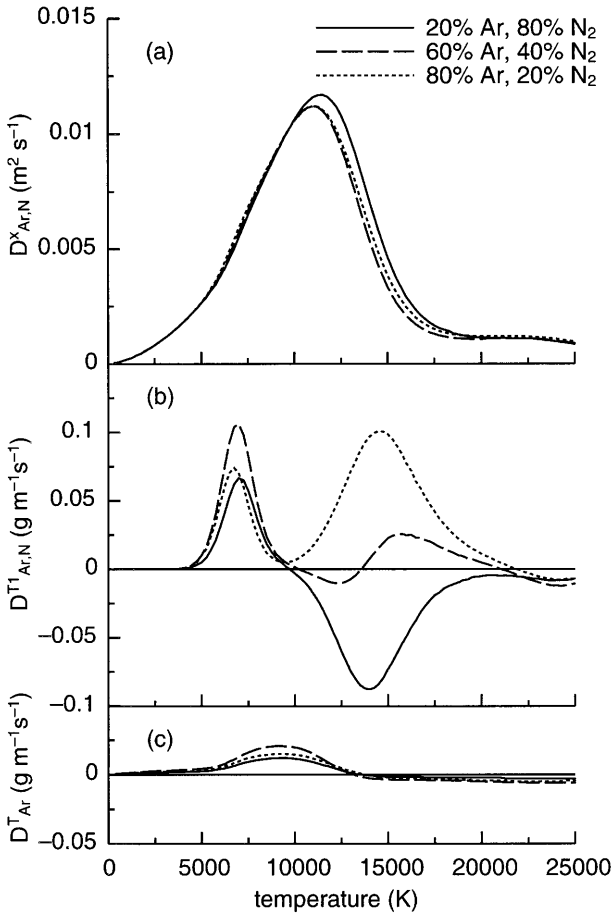

FIG. 10. Combined diffusion coefficients for different mixtures of argon and nitrogen by weight. (a) Combined mole fraction diffusion coefficient; (b) combined temperature diffusion coefficient; (c) combined thermal diffusion coefficient.

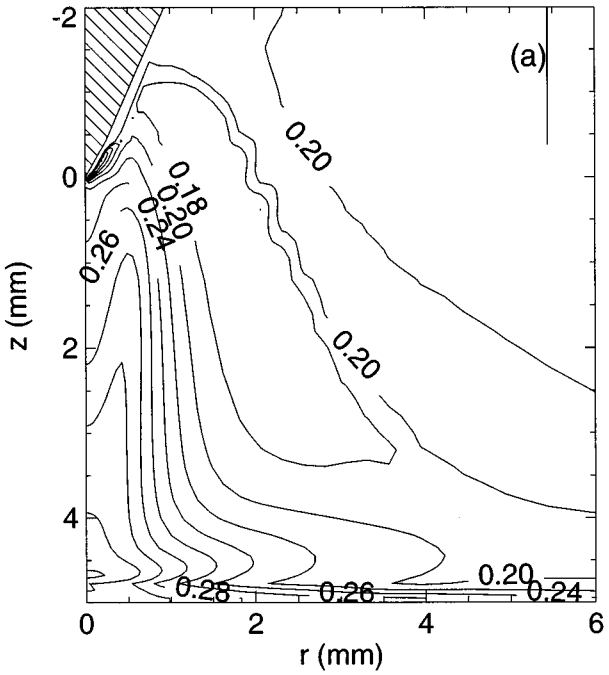

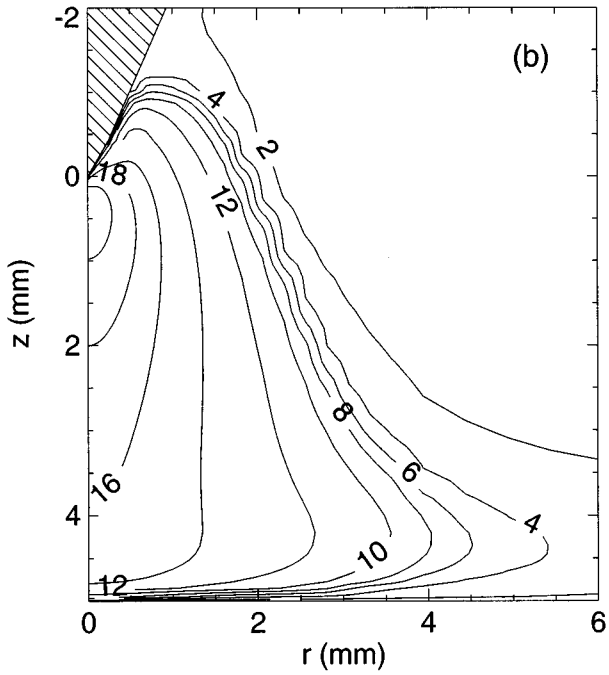

FIG. 11. (a) Isopleths of oxygen mass fraction and (b) isotherms, labeled in units of 1000 K; calculated for a 200 A 5 mm arc with a 10 L min^{-1} input flow composed of 20% oxygen and 80% argon by mass.

thermal diffusion on this occasion acts to decrease the hydrogen mass fraction near the arc axis. In all other gas mixtures considered, demixing due to thermal diffusion increased the mass fraction of the lighter gas in the high-temperature region. The change in direction of demixing due to thermal diffusion may be explained in terms of the combined thermal diffusion coefficient $\overline{D_{\mathrm{Ar}}^{T}}$, shown in Fig. 18. $\overline{D_{\mathrm{Ar}}^{T}}$ is negative at high temperatures, above about 10 000 K, for the mixtures of argon and hydrogen. In all other gas

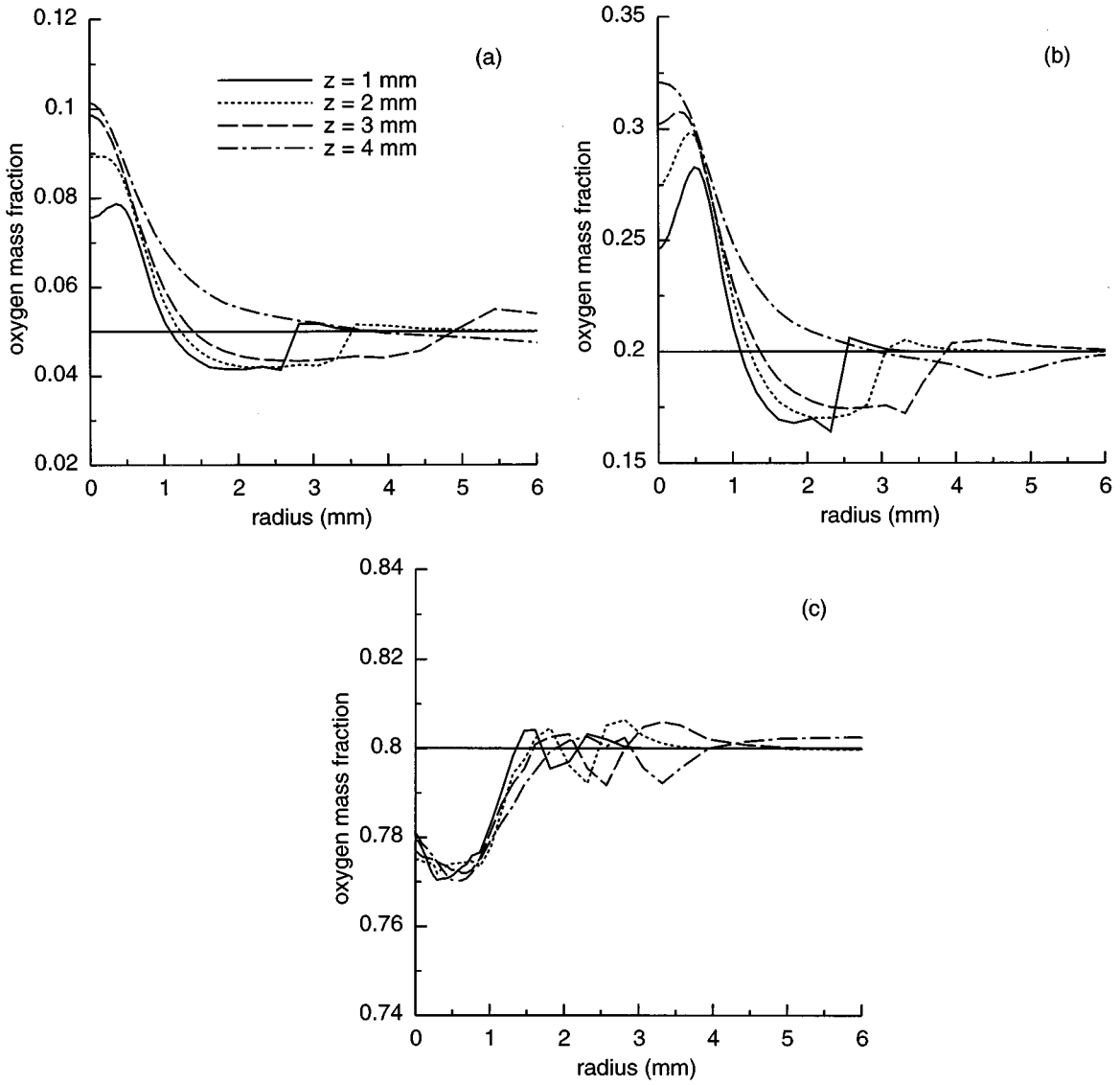

FIG. 12. Radial dependence of the mass fraction of oxygen gas at four axial distances below the cathode, for a 200 A 5 mm arc with a 10 L min^{-1} input flow composed of (a) 5% oxygen and 95% argon; (b) 20% oxygen and 80% argon; (c) 80% oxygen and 20% argon by mass. The horizontal line shows the input mass fraction.

mixtures considered, it is positive for almost the entire temperature range of interest. It is generally considered that the thermal diffusion coefficient of a heavy gas mixed with a lighter gas should be positive [53]; this is certainly the case at low temperatures, when only neutral species are present, but the present example shows that it is not necessarily true when ionized species are present.

Figure 18 also shows the other two combined diffusion coefficients for mixtures of argon and hydrogen. As noted above, they tend to be smaller, particularly at temperatures between 15 000 and 25 000 K, than for the argon-helium mixtures (cf. Fig. 6), despite the inverse dependence of diffusion coefficients with mass. The reason for this is that hydrogen ionizes at a lower temperature than helium, which means that the Coulomb interactions dominate at lower temperature. Diffusion coefficients depend inversely on the collision cross sections, and the Coulomb interaction has a much larger cross section than interactions between neutrals and between ions and neutrals.

The combined temperature diffusion coefficient $\overline{D^{T1}_{\mathrm{Ar,H}}}$ changes sign depending on the relative concentrations of the two gases, as did $\overline{D^{T1}_{\mathrm{Ar,N}}}$ and $\overline{D^{T1}_{\mathrm{Ar,O}}}$. The sign change occurs for a hydrogen mass fraction of about 0.15, corresponding to a mole fraction of around 0.8. This indicates that, despite the large mass difference between argon and hydrogen, arcs, demixing due to frictional forces will act in different directions depending on the mass fractions of the two gases, as was also seen in the argon-nitrogen and argon-oxygen arcs. Hence, in an arc containing a large percentage of hydrogen, the hydrogen mass fraction is expected to decrease below its input value near the arc axis.

It should be noted that it has been demonstrated that the density of hydrogen atoms in the fringe regions of argon-hydrogen arcs [35] is higher than that predicted assuming local chemical equilibrium. This is because the atoms diffuse more rapidly than they can recombine to form molecular hydrogen. However, this phenomenon only affects the com-

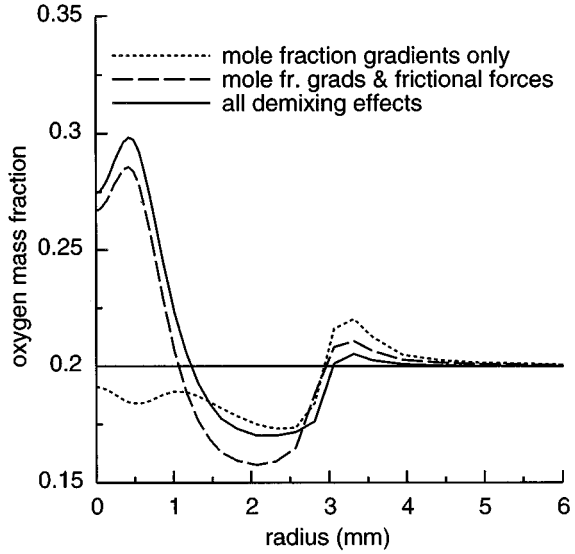

FIG. 13. Calculated radial dependence of the mass fraction of oxygen 2 mm below the cathode for the conditions of Fig. 11, with the effects of the different demixing processes shown.

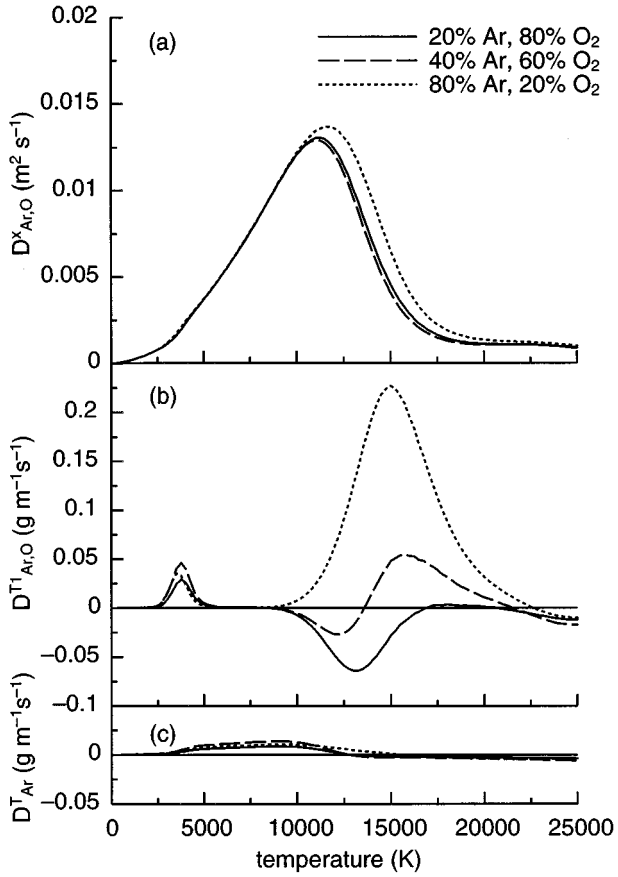

FIG. 14. Combined diffusion coefficients for different mixtures of argon and oxygen by weight. (a) Combined mole fraction diffusion coefficient; (b) combined temperature diffusion coefficient; (c) combined thermal diffusion coefficient.

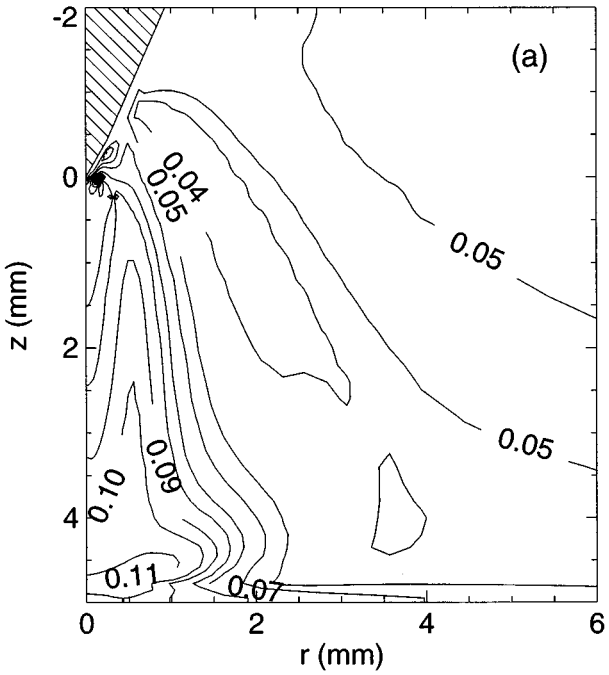

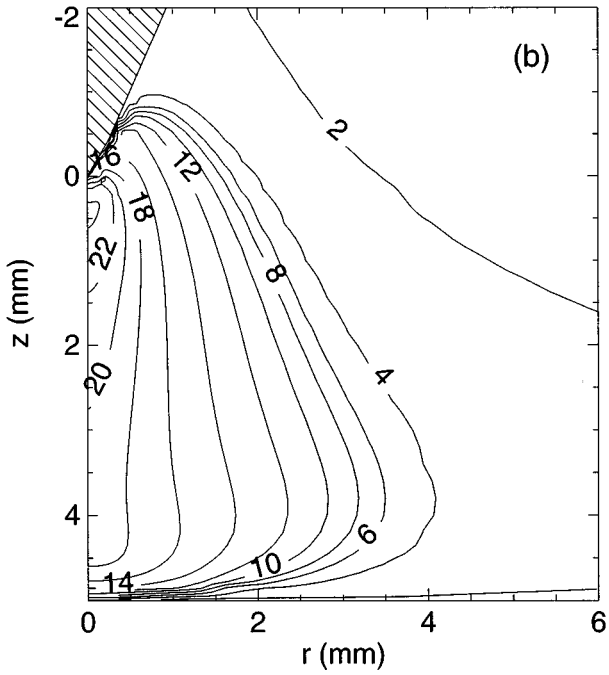

FIG. 15. (a) Isopleths of hydrogen mass fraction and (b) isotherms, labeled in units of 1000 K; calculated for a 200 A 5 mm arc with a 10 L min^{-1} input flow composed of 5% hydrogen and 95% argon by mass.

position in regions at temperatures lower than the recombination temperature of between 3000 and 3500 K. In these regions it may lead to a small increase in the hydrogen mass fraction over that calculated assuming local chemical equilibrium.

E. Effect of demixing on arc properties

It has been shown in Secs. III A–III D that demixing usually has a large effect on the composition of a free-

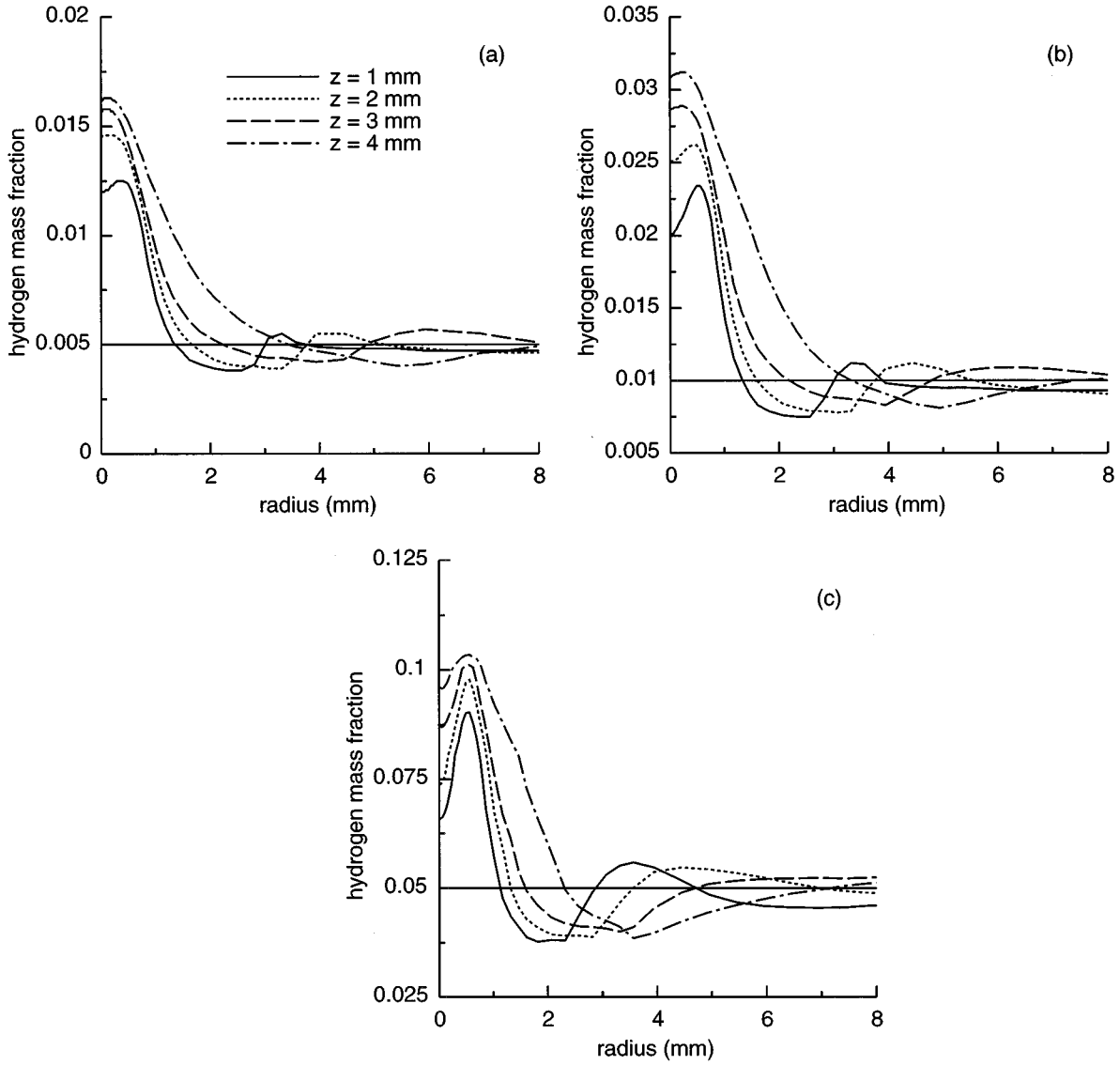

FIG. 16. Radial dependence of the mass fraction of hydrogen gas at four axial distances below the cathode, for a 200 A 5 mm arc with a 10 L min^{-1} input flow composed of (a) 0.5% hydrogen and 99.5% argon; (b) 1% hydrogen and 99% argon; (c) 5% hydrogen and 95% argon by mass. The horizontal line shows the input mass fraction.

burning arc. Here the effects of these changes in composition on three arc properties, the temperature, the axial flow velocity, and the heat flux to the anode, are considered.

Results for the first two of these properties are given in Table I. The temperature and the axial velocity on the arc axis are given for four axial positions for all the input gas compositions considered in Secs. III A–III D. Also given are the percentage changes in these properties due to the effect of demixing, calculated relative to the value of the property when the effect of demixing is neglected; i.e., assuming that the mass fraction of argon is everywhere equal to its input value. Temperatures and axial velocities for a pure argon arc are listed for comparison.

Despite the large changes in composition that demixing causes, it has only a relatively small influence on the arc temperature. The largest changes are in the argon-hydrogen mixtures, and even these are of order 6% or less. Figure 19 shows the temperature distribution calculated including and neglecting the effect of demixing for an arc in a mixture of 5% hydrogen and 95% argon by mass. Demixing decreases the arc temperature by 1450 K on axis 1 mm below the cathode; the changes are smaller elsewhere.

The influence of demixing on the flow velocity is also generally small. Typical changes are again less than 5%. However, in arcs in mixtures of argon and helium, including the influence of demixing in the calculations can decrease the axial velocity by more than 20%. The changes are larger close to the anode, as can be seen in Fig. 20, which shows the axial velocity distribution for an arc in a mixture of 10% helium and 90% argon by mass. This change is a result of the increase in viscosity with helium mass fraction that is calculated to occur in mixtures of argon and helium at high temperatures [47,54,55]; this is illustrated in Fig. 21, which shows viscosity for mixtures of argon and different gases. The increased helium mass fraction near the arc axis caused by demixing leads to a greater transfer of momentum from the central regions to the off-axis regions of the arc, leading to a less-peaked velocity profile. The effect is greater closer

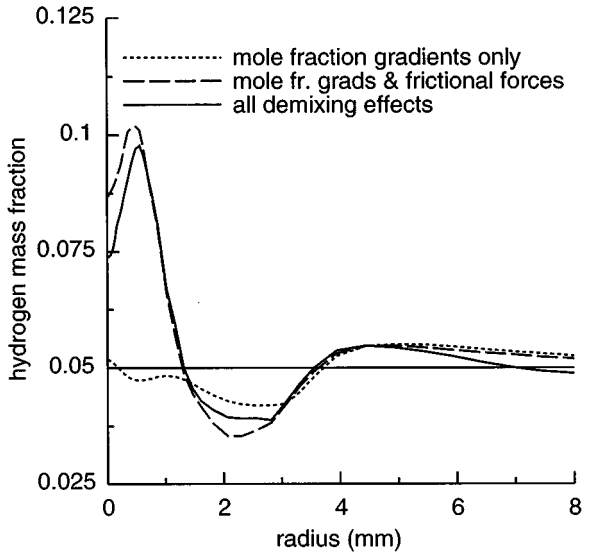

FIG. 17. Calculated radial dependence of the mass fraction of hydrogen 2 mm below the cathode for the conditions of Fig. 15, with the effects of the different demixing processes shown.

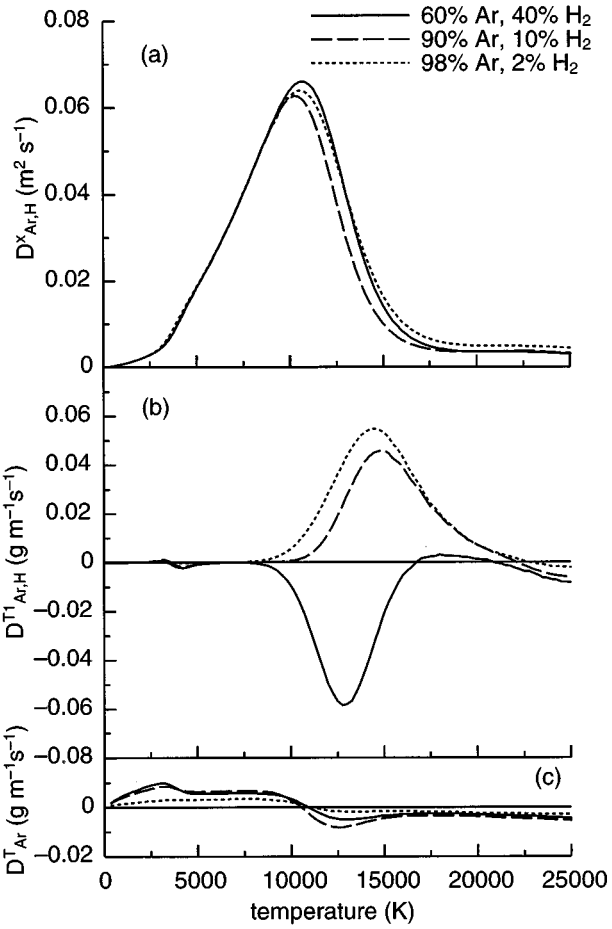

FIG. 18. Combined diffusion coefficients for different mixtures of argon and hydrogen by weight. (a) Combined mole fraction diffusion coefficient; (b) combined temperature diffusion coefficient; (c) combined thermal diffusion coefficient.

to the anode since the gas has traveled further to reach these positions. For the other gas mixtures, the viscosity is similar to that of pure argon, so the effect of demixing on the flow velocity is smaller.

Table I, as well as showing the influence of demixing on temperature and flow velocity, also shows some interesting trends in these quantities due to the addition of other gases to argon. The arc temperature and the axial velocity both increase as increasing proportions of the other gases are added to argon. The increase in the axial velocity is particularly dramatic. It may be attributed to the increase in the current density near the cathode, which leads to an increase in the magnetic pinch, or $\mathbf{j}\times\mathbf{B}$, force, the driving mechanism for the convective flow in the arc. The increase in current density is due to two effects. First, as shown in Fig. 22, the electrical conductivity is increased at the high temperatures ($\gtrsim$20 000 K) that are present near the cathode by the addition of one of the molecular gases. Second, the thermal conductivity is increased by the addition of one of the other gases, particularly the molecular gases, to argon, as shown in Fig. 23. The peaks at 3500 K for the argon-oxygen and argon-hydrogen mixtures and at 7000 K for the argon-nitrogen mixture are due to the reaction thermal conductivity associated with the dissociation of the molecular gases. The greater thermal conductivity causes the temperature profile of the arc to become more strongly peaked around the arc axis, which in turn leads to a higher current density near the cathode.

In many applications of free-burning arcs, such as GTAW welding, plasma cutting, and mineral processing, the role of the arc is to transfer a concentrated flux of heat to the anode. It is hence interesting to calculate the effect of demixing on the heat flux to the anode. The heat flux is the sum of the conduction term $-(\kappa/c_p)\partial h/\partial z$ and the electron heating term $-j_z\phi_a$, where j_z is the axial current density and ϕ_a is the anode work function, taken to be 4.65 V. Zhu *et al.* [56] have shown that other terms are negligible. The anode temperature profile is taken to be that calculated by Zhu *et al.* for a 5 mm thick copper anode and a 200 A argon arc. The axial dimension of the grid adjacent to the anode is chosen to be 0.1 mm. It is important not to make this dimension smaller than the anode sheath thickness, shown by Morrow and Lowke [57] to be typically about 0.04 mm, since in this region transport is dominated by electron diffusion and the local thermodynamic equilibrium (LTE) approximation used in the code is not valid. Decreasing the dimension below 0.04 mm leads to unrealistically high values of the arc voltage and the total anode heat flux, whereas decreasing the dimension from 0.1 to 0.05 mm leads to only a 5% change in these quantities. The trends observed in the radial profile of the anode heat flux are not significantly altered by decreasing the dimension from 0.1 to 0.05 mm.

Figure 24 shows the heat flux to the anode, calculated including and neglecting the influence of demixing, for arcs in mixtures of argon and helium, nitrogen, oxygen, and hydrogen. Demixing has a very large influence in the argon-hydrogen arc, increasing the heat flux by the order of 50% on axis. Similar increases were calculated for the 1% and 0.5% hydrogen arcs. A smaller increase, about 10%, is found for the argon-nitrogen arc. The increases are mainly in the conductive component, and may be explained by the increased

TABLE I. Temperature and axial velocity on axis, at four axial positions below the cathode, for arcs in mixtures of argon and different mass fractions of other gases. The percentage changes in the temperatures and axial velocities relative to their values calculated neglecting the effect of demixing are also given. Results for pure argon are given for comparison.

Gas	Mass fraction	Temperature (K)				Axial velocity ($m\ s^{-1}$)			
		1 mm	2 mm	3 mm	4 mm	1 mm	2 mm	3 mm	4 mm
He	0.01	19940	18500	17310	16500	374	377	356	283
		1.9%	0.6%	−0.3%	−0.5%	0.6%	−1.4%	−3.1%	−5.8%
He	0.05	20440	19680	18640	17500	417	386	330	222
		−0.2%	2.2%	3.9%	3.4%	2.0%	−2.5%	−7.4%	−15.6%
He	0.10	20310	19750	19140	18320	445	392	312	175
		−1.6%	0.9%	2.5%	4.7%	3.8%	−1.8%	−8.3%	−21.3%
N_2	0.20	21080	18470	16900	16000	570	587	570	496
		−2.3%	−2.3%	−1.6%	−1.2%	−1.8%	−1.5%	−1.5%	−2.4%
N_2	0.45	22880	19590	17450	16340	835	842	809	716
		0.1%	0.2%	0.1%	0.0%	2.2%	1.8%	1.6%	1.5%
N_2	0.75	24910	21600	18600	17060	1067	1067	1027	928
		1.3%	4.0%	2.3%	1.0%	−7.6%	−7.6%	−7.7%	−7.9%
O_2	0.05	19650	18070	16950	16170	392	409	398	333
		−1.9%	−1.7%	−1.5%	−1.5%	−0.7%	−0.8%	−1.3%	−3.2%
O_2	0.20	19940	18000	16770	15930	488	499	475	390
		−4.1%	−3.9%	−3.2%	2.9%	−4.5%	−2.4%	−3.1%	−6.1%
O_2	0.80	22940	19890	18030	16840	900	889	840	724
		0.7%	0.9%	0.7%	0.2%	−0.3%	−0.4%	−0.3%	0.1%
H_2	0.005	19920	18420	17360	16680	482	502	490	422
		−6.2%	−4.7%	−5.8%	−2.7%	−1.1%	0.0%	−0.3%	−2.5%
H_2	0.01	20860	19380	18170	17430	592	613	598	518
		−5.1%	−2.7%	−1.4%	1.1%	0.1%	1.6%	1.8%	−1.4%
H_2	0.05	22970	21070	19630	18820	1182	1173	1122	989
		−5.9%	−2.5%	0.2%	−0.8%	−0.5%	−0.1%	1.5%	0.0%
Ar only		19350	17960	16940	16240	348	366	358	300

thermal conductivity of the gas mixture in the temperature range present close to the anode, between about 5000 and 10 000 K. Figure 23 shows that the presence of hydrogen or nitrogen greatly increases the thermal conductivity for temperatures below 10 000 K, far more than for the other gases considered. Hence the conduction to the anode near the arc axis is strongly increased by the increase in hydrogen or nitrogen concentration caused by demixing. The effect is larger for hydrogen since demixing causes a greater increase in mass fraction than for nitrogen.

The addition of oxygen only has a large influence on the thermal conductivity at temperatures up to around 5000 K. Such temperatures are only present within the sheath region. No attempt is made here to treat the sheath region, so it is not possible to conclude whether the reaction component of the thermal conductivity arising from the dissociation of oxygen molecules will have a significant effect on the anode heat flux. Nevertheless, the effect is expected to be much smaller than that observed for argon-hydrogen arcs.

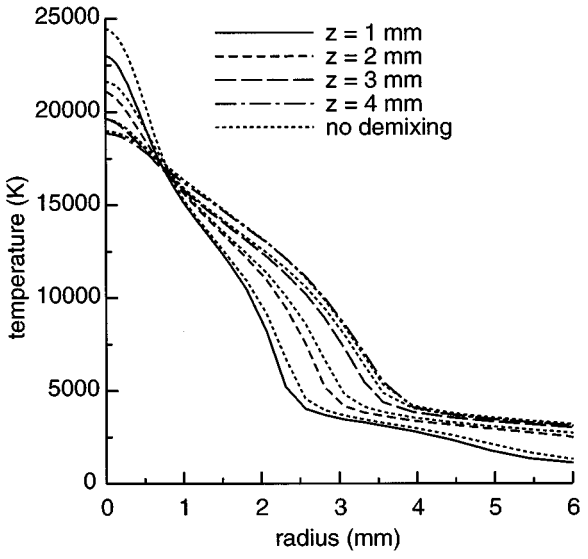

FIG. 19. Radial dependence of temperature at four axial distances below the cathode for a 200 A 5 mm arc with a 10 L min^{-1} input flow composed of 5% hydrogen and 95% argon by mass. The dotted lines show values calculated neglecting demixing, while the other line types show values calculated including the effects of demixing.

IV. COMPARISON WITH EXPERIMENT

The mass fraction of nitrogen has been measured in arcs in different mixtures of argon and nitrogen using a spectroscopic technique [58] that is an extension of the Fowler-Milne method. The technique requires the emission from a

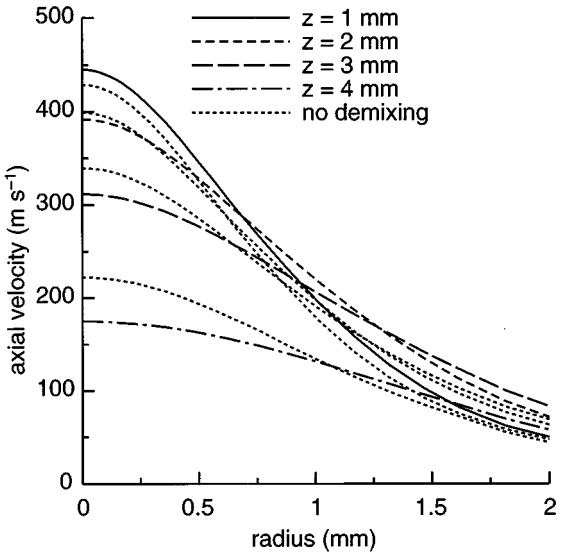

FIG. 20. Radial dependence of axial velocity at four axial distances below the cathode for a 200 A 5 mm arc with a 10 L min^{-1} input flow composed of 10% helium and 90% argon by mass. The dotted lines show values calculated neglecting demixing, while the other line types show values calculated including the effects of demixing.

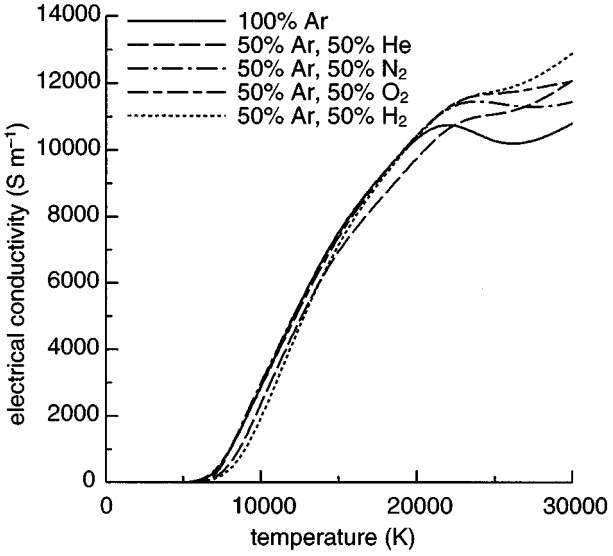

FIG. 22. Dependence of electrical conductivity on temperature for argon and mixtures of 50% argon and 50% helium, nitrogen, oxygen, and hydrogen by mole fraction.

neutral argon line and from a neutral nitrogen line to be measured. The radial dependence of the emission coefficients is obtained through an Abel transform of the data.

The method is applicable only to regions in local thermodynamic equilibrium, which, as shown by Cram *et al.* [59], means that data cannot be obtained for those regions at temperatures below around 11 000 K. Also, the errors that result from the Abel transform procedure accumulate in the center of the arc, meaning that uncertainties are so large in the central 0.2 mm that mass fractions cannot be determined. In the remaining regions, the uncertainty in the mass fraction is less than about 0.02. This uncertainty corresponds to the amplitude of the small scale oscillations with spatial period of about 0.2 mm that appear in some of the mass fraction data; these oscillations are also an artifact of the Abel transform procedure.

Figure 25 shows the radial dependence of the mass fraction of nitrogen at four axial positions for an arc in a mixture of 22% nitrogen and 78% argon by mass. The measured data are compared to the predictions of the model for the same conditions. The agreement is found to be good, with the measured increase in the nitrogen mass fraction as temperature increases being well reproduced by the model.

Measurements were also made for argon-nitrogen mixtures containing 41% and 68% nitrogen by mass. The mass

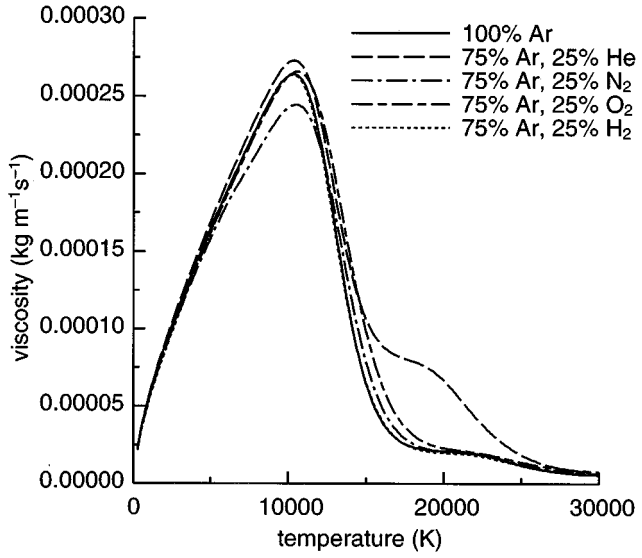

FIG. 21. Dependence of viscosity on temperature for argon and mixtures of 75% argon and 25% helium, nitrogen, oxygen, and hydrogen by mole fraction.

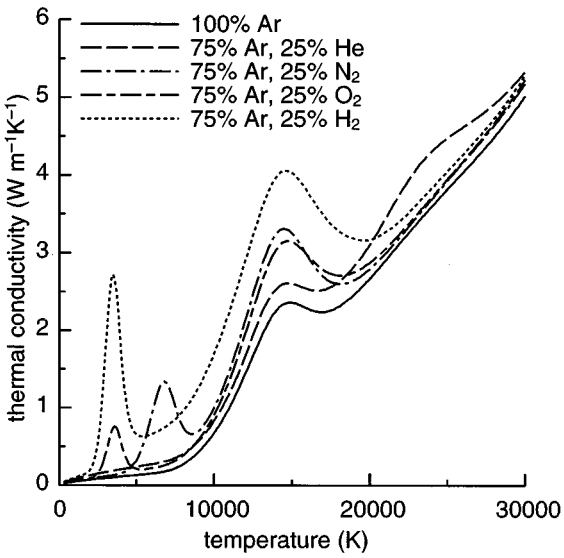

FIG. 23. Dependence of thermal conductivity on temperature for argon and mixtures of 75% argon and 25% helium, nitrogen, oxygen, and hydrogen by mole fraction.

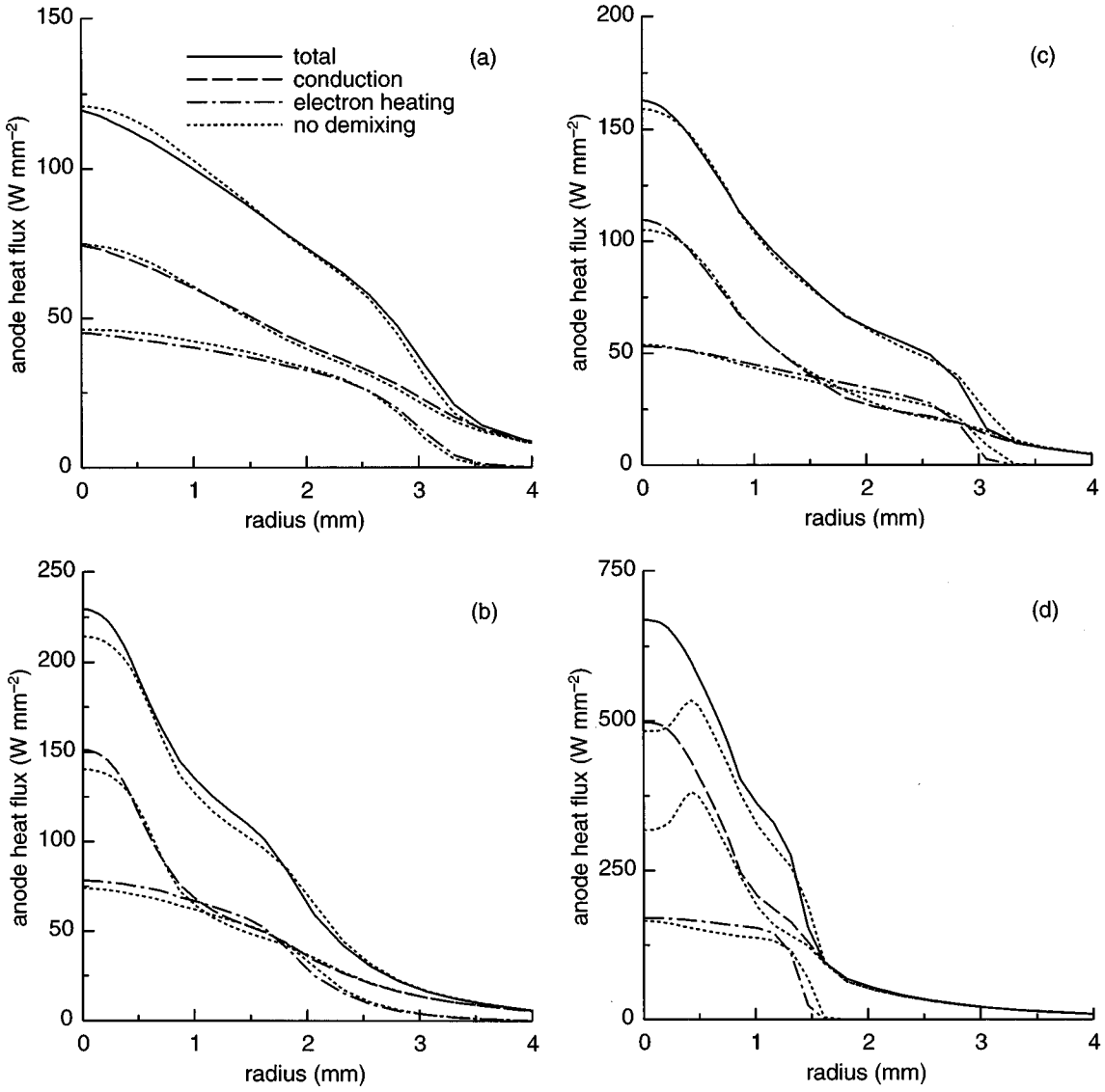

FIG. 24. Radial dependence of the heat flux to the anode in 200 A 5 mm arcs with a 10 L min^{-1} input flow composed of (a) 10% helium and 90% argon, (b) 20% nitrogen and 80% argon, (c) 20% oxygen and 80% argon, (d) 5% hydrogen and 95% argon, by mass. The contributions due to conduction and electron heating are shown separately. The dotted lines show values calculated neglecting demixing, while the other line types show values calculated including the effects of demixing.

fractions and temperatures measured along a radius 1 mm below the cathode are shown in Fig. 26 for the three gas mixtures. Good agreement with the predictions of the model is again found. In particular, the change in direction of demixing as the proportion of nitrogen in the gas mixture is increased is also shown by the measured data. Unfortunately, owing to the limitations of the measurement technique that were noted above, the influence of the convective flow close to the arc axis, and the demixing effects in the region in which nitrogen molecules dissociate, could not be checked experimentally.

Some measurements of helium mass fraction in an argon-helium arc have been presented by Hiraoka [32], who used a spectroscopic technique that involved the measurement of the emission from an Ar I and an Ar II line to find the helium concentration on the axis of arcs in different mixtures of argon and helium. The measurements were made in an arc with different parameters from those considered thus far. The arc current was 100 A, the cathode had the same diameter (3.2 mm) but the tip had an included angle of 45°, and the distance between the cathode tip and the anode was 3 mm. The model has been used to simulate an arc with these parameters for the same mixtures of argon and helium that were considered in Sec. III A. Hiraoka did not specify the input gas flow rate, and 10 L min^{-1} has again been used. Typical results are shown in Fig. 27. Comparison with the results for the 200 A 5 mm arc shown in Fig. 3 shows that the maximum value of the helium mass fraction is smaller in the 100 A arc; this is a result of the smaller temperature gradients in the central region of the arc. The predictions of the model are compared with Hiraoka's measurements of the helium mass fraction 1 mm below the cathode on the arc axis in Fig. 28. Once again, close agreement is found with the experimental data.

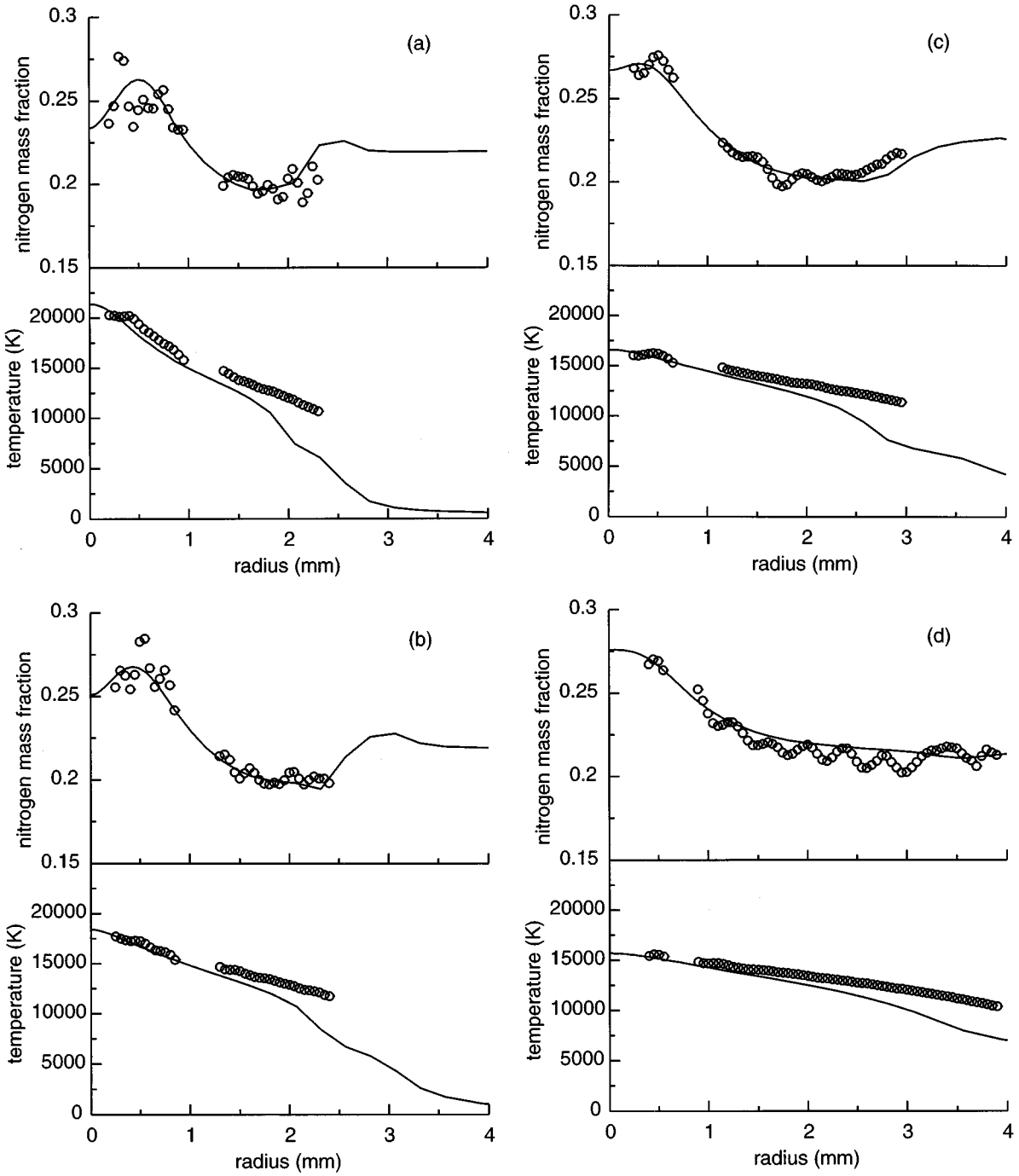

FIG. 25. Radial dependence of the mass fraction of nitrogen and temperature at positions (a) 1 mm, (b) 2 mm, (c) 3 mm, and (d) 4 mm below the cathode in a 200 A 5 mm free-burning arc with a 11.0 L min^{-1} input flow composed of 22% nitrogen and 78% argon by mass. ○, spectroscopic measurements; —, calculations.

V. CONCLUSIONS

A numerical model of a free-burning arc in a mixture of two gases has been developed. The key innovation in the model is the use of the combined diffusion coefficient concept to treat the diffusion of the two gases. This has allowed the phenomenon of demixing to be treated simply yet accurately, under the assumption of local chemical equilibrium.

The model has been applied to investigate demixing in mixtures of argon with helium, nitrogen, oxygen, and hydrogen; all these mixtures are used in industrial arc processes.

The effects of demixing on the composition of the arc have been shown to be large in most cases. The greatest effect was found in the argon-hydrogen arc, for which it was found that the hydrogen mass fraction could be increased by a factor of more than 3 on the arc axis. The smallest effect was for the argon-nitrogen arc, but even in this case the nitrogen mass fraction could be increased by 25% near the arc axis. Only for narrow ranges of compositions of mixtures of argon and nitrogen, argon and oxygen, and argon and hydrogen, is the effect of demixing small. Usually, but not always, the effect of demixing on the composition was found to be greater for a greater mass difference between the two gases.

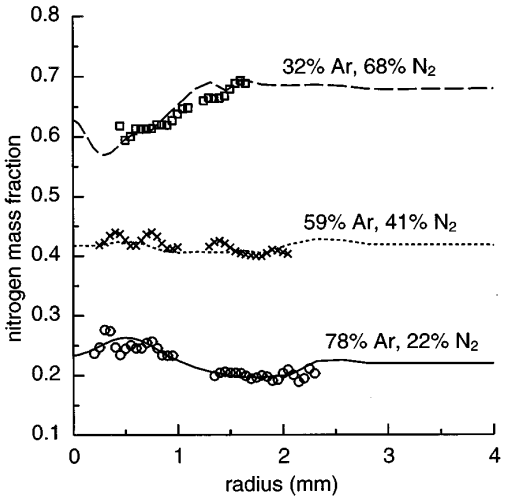

FIG. 26. Radial dependence of the mass fraction of nitrogen at a position 1 mm below the cathode in 200 A 5 mm free-burning arcs in mixtures of argon and nitrogen. Measurements are shown by symbols and calculations by curves. ○, —, 78% argon, 22% nitrogen, 11.0 L min^{-1} total flow; ×, ···, 59% argon, 41% nitrogen, 10.5 L min^{-1} total flow; □, − − −, 32% argon, 68% nitrogen, 10.1 L min^{-1} total flow; all proportions are by mass.

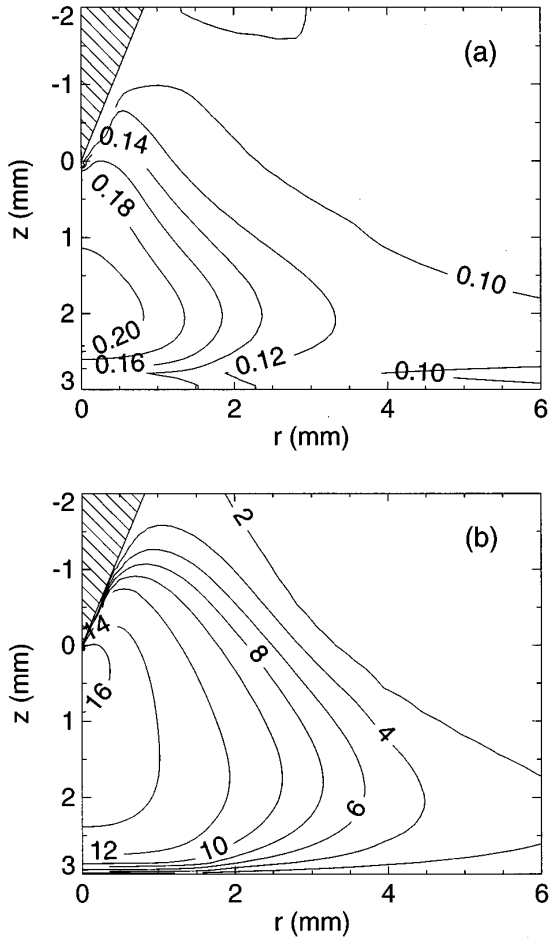

FIG. 27. (a) Isopleths of helium mass fraction and (b) isotherms, labeled in units of 1000 K; calculated for a 100 A 3 mm arc with an included cathode angle of 45°. The input gas flow is 10 L min^{-1}, composed of 10% helium and 90% argon by mass.

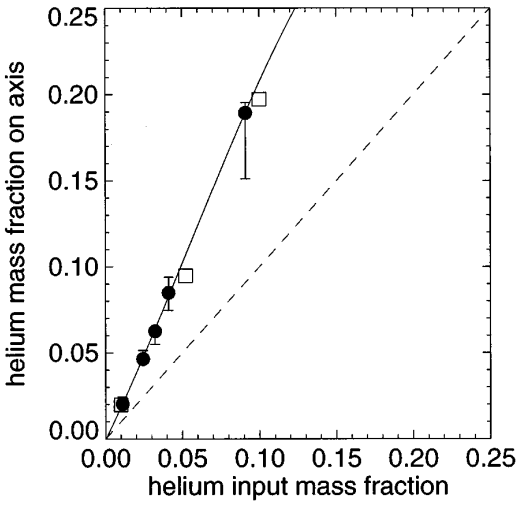

FIG. 28. Mass fraction of helium on axis, 1 mm below the cathode, plotted against the mass fraction of helium in the input gas mixture, for 100 A 3 mm arcs with a 10 L min^{-1} input flow. ●, spectroscopic measurements presented by Hiraoka [32]; □, calculations. The dotted line represents the hypothetical case of no demixing, and the solid line is a fit to Hiraoka's measurements.

Complicated mass fraction distributions were observed for arcs in mixtures of argon with molecular gases, because different demixing processes act in opposite directions in regions at different temperatures. It has been shown, however, that the mass fraction distributions are readily explicable in terms of three different demixing processes and the influence of the convective, or mass-average, flow. The first demixing process, demixing due to mole fraction gradients, occurs in regions at temperatures at which a gas ionizes or dissociates. It leads to a displacement of that gas from regions at higher temperature to regions at lower temperature than the ionization or dissociation temperature. The second demixing process, demixing due to frictional forces, typically causes a displacement of the lighter gas to regions at high temperature, although it has been shown that in the case of argon-nitrogen, argon-oxygen, and argon-hydrogen mixtures, it may act in either direction depending on the relative mass fractions of the two gases. The final demixing process, demixing due to thermal diffusion, has only a minor influence on the arc composition. It usually, but not always, acts to concentrate the lighter gas in regions of high temperature. The influence of the convective flow of fully mixed gas from around the cathode into the arc is to oppose the effect of demixing; however, convection is only effective within 1 mm or less of the arc axis, and even then not for mixtures containing helium, which diffuses very rapidly.

Use of the combined diffusion coefficient formulation to treat diffusion between the two gases allows the effect of three demixing processes to be separated, since each of the three combined diffusion coefficients corresponds to a different demixing process. In particular, knowledge of the sign of the combined temperature and thermal diffusion coefficients allows the direction of demixing due to frictional forces and due to thermal diffusion, respectively, to be predicted. It is found that the most important demixing process in the high-temperature regions, where the gases are dissociated and at

least partially ionized, is demixing due to frictional forces. The other two demixing processes can also have significant influences in these regions. In the regions at lower temperature, where dissociation of molecular gases occurs, demixing due to mole fraction gradients is the dominant process.

Despite the large changes in composition caused by demixing, there is only a relatively small effect on arc temperature and flow velocity. Changes of less than 5% are typically calculated. Only in the case of the velocity near the axis of argon-helium arcs does including demixing in the calculations have an effect of more than 10%. However, the heat flux to the anode is significantly increased near the axis by demixing in the argon-nitrogen and particularly in the argon-hydrogen arcs. The changes in flow velocity and anode heat flux can be explained in terms of the material properties of the gas mixtures.

The predictions of the numerical model have been compared with spectroscopic measurements of mass fraction distributions in argon-nitrogen arcs and of the mass fraction on axis in argon-helium arcs. Good agreement has been demonstrated between the measurements and the calculations. In particular, the change in the direction of demixing that has been predicted in the argon-nitrogen arc as the fraction of nitrogen in the input gas mixture was increased was verified by the experiments. Further, the magnitude of the change in mass fraction predicted to be caused by demixing is verified by the measurements.

Mixtures of gases are used for two main reasons in arc and plasma processes; first, to provide the species required to drive chemical reactions in the arc or at the electrodes, and second, to increase thermal transport to the electrodes or to particles injected into the plasma. The results of this study have shown that demixing generally causes large changes in the composition of an arc, and that, in some mixtures, significant changes in flow velocity and thermal transport result. Hence both the chemical and thermal processes occurring in the arc can be influenced by demixing. It may be concluded that it is important to consider the effects of demixing when modeling arc and plasma processes that employ mixtures of gases.

[1] P. Lenard, Ann. Phys. (Leipzig) **11**, 636 (1903).
[2] A. Eberhagen, Z. Phys. **143**, 312 (1955).
[3] Cataphoresis may be classified as a demixing process, driven by the electric field; however, it is not considered further in this paper.
[4] R. Mannkopf and C. Peters, Z. Phys. **70**, 444 (1931).
[5] R. Mannkopf, Z. Phys. **76**, 396 (1932).
[6] R. Mannkopf, Z. Phys. **86**, 161 (1933).
[7] W. Frie, Z. Phys. **172**, 99 (1963).
[8] H. Maecker, Ann. Phys. (Leipzig) Ser. 6 **18**, 441 (1956).
[9] F. Mastrup and W. Wiese, Z. Astrophys. **44**, 259 (1958).
[10] O. Roder, Z. Astrophys. **55**, 38 (1962).
[11] K. H. Wobig, Z. Astrophys. **55**, 100 (1962).
[12] J. B. Schumaker, Jr. and C. H. Popenoe, Phys. Rev. Lett. **21**, 1046 (1968).
[13] E. Schulz-Gulde, Z. Phys. **245**, 308 (1971).
[14] G. Baruschka and E. Schulz-Gulde, Astron. Astrophys. **44**, 335 (1975).
[15] W. Frie, Z. Phys. **162**, 61 (1961).
[16] W. Frie and H. Maecker, Z. Phys. **162**, 69 (1961).
[17] W. Frie and H. Maecker, Z. Phys. **168**, 206 (1962).
[18] J. Richter, Z. Astrophys. **53**, 262 (1961).
[19] H. Motschmann, Z. Phys. **200**, 93 (1967).
[20] H. Motschmann, Z. Phys. **214**, 42 (1968).
[21] E. Schulz-Gulde, J. Phys. D **13**, 793 (1980).
[22] S. Vacquié, High Temp. Chem. Process. **3**, 613 (1994).
[23] J. J. Gonzalez, J. B. Belhaouari, and A. Gleizes, J. Phys. D **29**, 1520 (1996).
[24] D. Vukanović, Spectrochim. Acta **22**, 815 (1966).
[25] D. Vukanović and V. Vukanović, Spectrochim. Acta **24B**, 579 (1969).
[26] E. Fischer, J. Appl. Phys. **47**, 2954 (1976).
[27] H.-P. Stormberg, J. Appl. Phys. **52**, 3233 (1981).
[28] D. Karabourniotis, E. Drakakis, and A. Palladas, J. Phys. D **27**, 781 (1994).
[29] B. Cheminat, R. Gadaud, and P. Andanson, J. Phys. D **20**, 444 (1987).
[30] W. D. Swank, J. R. Fincke, and D. C. Haggard, Rev. Sci. Instrum. **64**, 56 (1993).
[31] J. R. Fincke, C. H. Chang, W. D. Swank, and D. C. Haggard, Int. J. Heat Mass Transfer **37**, 1673 (1994).
[32] K. Hiraoka, in *Proceedings of the 11th International Symposium on Plasma Chemistry, Loughborough, England, 1993*, edited by J. E. Harry (Int. Union Pure & Appl. Chem., Oxford, 1993), Vol. 1, p. 440.
[33] A. M. Fudolig, H. Nogami, and J. Yagi, Iron Steel Inst. Jpn. Int. **36**, 1222 (1996).
[34] M. Suzuki, Y. Sato, and H. Akatsuka, Plasma Chem. Plasma Process. **16**, 399 (1996).
[35] S. C. Snyder, A. B. Murphy, D. L. Hofeldt, and L. D. Reynolds, Phys. Rev. E **52**, 2999 (1995).
[36] A. B. Murphy, Phys. Rev. E **48**, 3594 (1993); **50**, 5145(E) (1994).
[37] A. B. Murphy, Phys. Rev. Lett. **73**, 1797 (1994).
[38] A. B. Murphy, Pure Appl. Chem. **68**, 1137 (1996).
[39] A. B. Murphy, Appl. Phys. Lett. **69**, 328 (1996).
[40] J. O. Hirschfelder, C. F. Curtiss, and R. B. Bird, *Molecular Theory of Gases and Liquids*, 2nd ed. (Wiley, New York, 1964).
[41] R. S. Devoto, Phys. Fluids **9**, 1230 (1966).
[42] A. B. Murphy, J. Phys. D **29**, 1922 (1996).
[43] J. J. Lowke, P. Kovitya, and H. P. Schmidt, J. Phys. D **25**, 1600 (1992).
[44] P. Kovitya, IEEE Trans. Plasma Sci. **PS-12**, 38 (1984).
[45] S. Gordon and B. J. McBride, NASA Report No. SP-273, 1971 (unpublished).
[46] A. B. Murphy and C. J. Arundell, Plasma Chem. Plasma Process. **14**, 451 (1994).
[47] A. B. Murphy, IEEE Trans. Plasma Sci. (to be published).
[48] L. E. Cram, J. Phys. D **18**, 401 (1985).
[49] K. A. Ernst, J. G. Kopainsky, and H. H. Maecker, IEEE Trans. Plasma Sci. **1**, No. 4, 3 (1973).
[50] V. Aubrecht and J. J. Lowke, J. Phys. D **27**, 2066 (1994).

[51] S. V. Patankar, *Numerical Heat Transfer and Fluid Flow* (Hemisphere, Washington, DC, 1980).
[52] J. P. Van Doormaal and G. D. Raithby, Numer. Heat Transfer **7**, 147 (1984).
[53] W. H. Furry, Am. J. Phys. **16**, 63 (1948).
[54] B. Pateyron, M.-F. Elchinger, G. Delluc, and P. Fauchais, Plasma Chem. Plasma Process. **12**, 421 (1992).
[55] W. L. T. Chen, J. Heberlein, E. Pfender, B. Pateyron, G. Delluc, M. F. Elchinger, and P. Fauchais, Plasma Chem. Plasma Process. **15**, 559 (1995).
[56] P. Zhu, J. J. Lowke, R. Morrow, and J. Haidar, J. Phys. D **28**, 1369 (1995).
[57] R. Morrow and J. J. Lowke, J. Phys. D **26**, 634 (1993).
[58] A. B. Murphy, Rev. Sci. Instrum. **65**, 3423 (1994).
[59] L. E. Cram, L. Poladian, and G. Roumeliotis, J. Phys. D **21**, 418 (1988).